

Correlation between domain behavior and magnetic properties of materials

by

Jeffrey Scott Leib

A thesis submitted to the graduate faculty
in partial fulfillment of the requirements for the degree of
MASTER OF SCIENCE

Major: Materials Science and Engineering

Program of Study Committee:
David Jiles (Major Professor)
Vitalij Pecharsky
Vikram Dalal

Iowa State University

Ames, Iowa

2003

Copyright © Jeffrey Scott Leib, 2003. All rights reserved.

Graduate College
Iowa State University

This is to certify that the master's thesis of
Jeffrey Scott Leib
has met the thesis requirements of Iowa State University

David J. Jorgensen

Major Professor

For the Major Program

TABLE OF CONTENTS

1. INTRODUCTION AND BACKGROUND	1
2. CASE STUDIES: INTRODUCTIONS AND EXPERIMENTAL METHODS	7
2.1 CASE STUDY 1: Stress in an FeSiAl thin film resulting in stripe domains	7
2.2 CASE STUDY 2: Magnetization reversal in CoFeHfO films	9
2.3 CASE STUDY 3: Anisotropy in a Complex Magnetic Material	10
2.4 CASE STUDY 4: Melt-spun Fe ₇₅ Si ₁₀ B ₁₅ Ribbons	13
2.5 CASE STUDY 5: Magnetic Tunnel Junction Behavior	13
3. RESULTS	
3.1 CASE STUDY 1: Stress in an FeSiAl thin film resulting in stripe domains	17
3.2 CASE STUDY 2: Magnetization reversal in CoFeHfO films	22
3.3 CASE STUDY 3: Anisotropy in a Complex Magnetic Material	26
3.4 CASE STUDY 4: Melt-spun Fe ₇₅ Si ₁₀ B ₁₅ Ribbons	29
3.5 CASE STUDY 5: Magnetic Tunnel Junction Behavior	31
4. DISCUSSION	
4.1 CASE STUDY 1: Stress in an FeSiAl thin film resulting in stripe domains	34
4.2 CASE STUDY 2: Magnetization reversal in CoFeHfO films	37
4.3 CASE STUDY 3: Anisotropy in a Complex Magnetic Material	38
4.4 CASE STUDY 4: Melt-spun Fe ₇₅ Si ₁₀ B ₁₅ Ribbons	40
4.5 CASE STUDY 5: Magnetic Tunnel Junction Behavior	41
5. CONCLUSIONS	43
6. WORKS CITED	46
APPENDIX: COPIES OF PUBLICATIONS AND PAPERS	48

1. INTRODUCTION AND BACKGROUND

Correlation between length scales in the field of magnetism has long been a topic of intensive study. The long-term desire is simple: to determine one theory that completely describes the magnetic behavior of matter from an individual atomic particle all the way up to large masses of material. One key piece to this puzzle is connecting the behavior of a material's domains on the nanometer scale with the magnetic properties of an entire large sample or device on the centimeter scale.

The task of explaining the bulk properties of both ferromagnetic and paramagnetic materials was, in fact, the driving force for the initial formulation of domain theory. The initial debate was over the existence of atomic magnetic moments themselves, with evidence eventually accumulating in favor of what were then called "molecular magnets" [1]. In fact, Ampere postulated that these molecular magnets were due to atomic electrical currents similar to electromagnets, about 75 years before the discovery of the electron [1] and that these currents were permanent even without an external field applied. Over time, pieces to the puzzle began falling into place, including an explanation of paramagnetism based on atomic moment theory by Langevin [2], discovery of the discontinuous nature of the hysteresis loop by Barkhausen, formulation of the idea that a "magnetic" material might have saturated domains oriented randomly to add to zero when demagnetized, and finally in the 1920's and 1930's the idea of domains with finite transition regions called walls, consisting of magnetic moments whose orientations varied across the length of the wall [3].

The actual magnetic domain structures are due to the need for the magnetic material's desire to minimize magnetostatic energy at the cost of formation of the domain walls. As a

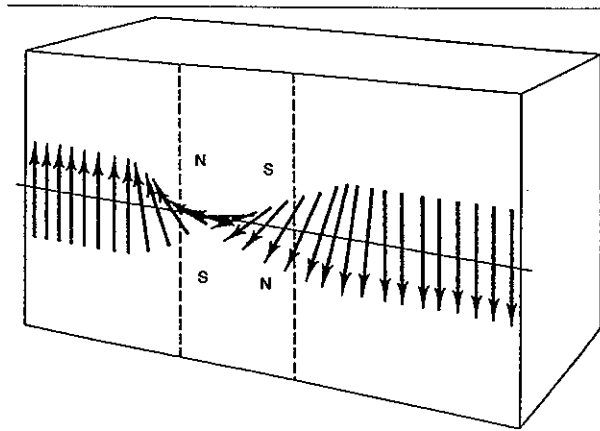


Fig. 1: Rotation of individual moments within a 180° domain wall [1].

ferromagnetic material consisting of one

bulk domain will have the energy

$$E = \frac{\mu_0}{2} N_d M^2$$

(where N_d is the

demagnetizing factor and M the

magnetization), the natural response of the

system will be to minimize M [1]. This is

accomplished via large groups of collinear

moments, usually pointing in favorable

crystallographic directions, with domain walls in which the magnetization vectors rotate from one group's direction to another. If the material is demagnetized or has spontaneously magnetized passing through a Curie point, the total magnetostatic energy of the system can be zero, at the cost of the energy bound in the force required to maintain misorientation of moments in the domain walls. Moment rotation usually increments toward vectors 180° or 90° from the original, as seen in Fig. 1, with the width and number of walls dependent on the strength of exchange and strength of crystalline anisotropy [1]. As many of the interesting properties of ferromagnetic materials derive from the movement, creation, or annihilation of these domain walls, there should be a strong correlation between what is seen at the domain scale and bulk magnetic measurements such as hysteresis curves.

Unfortunately, the initial difficulty of domain imaging and the inherently complicated nature of domains have both retarded progress in their understanding. Initial attempts at viewing domains involved dispersion of ultra-fine iron or magnetite particles on a polished surface, a process that soon evolved into the distribution of a magnetic particle colloid instead of powders. The first published work using this idea came from Bitter [4] and has since been known as the Bitter method. The resolution of the technique has been as good or better than the optical microscopes used to view the patterns, but neither the sensitivity nor repeatability of the technique are reliable and often depend on the skill of the individual researcher. Also, attempts to quantify results by counting particles at boundaries and using complicated models largely failed [5]. A more practical method of imaging domains takes advantage of the Kerr effect, where polarized light waves will have their direction of polarization rotated by magnetic fields at the surface of magnetic materials. In Kerr microscopy, the direction and magnitude of rotation will depend on the direction of the magnetic field with respect to the direction of the incident light beam. This fact that has led to the development of one of the first quantitative methods for domain analysis by Hubert and co-workers [5]. This method

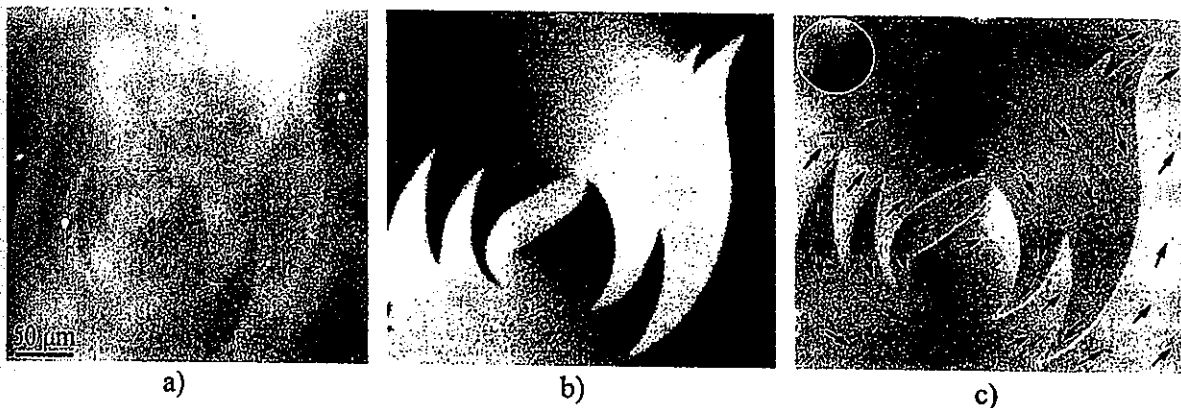


Fig. 2: a) A Kerr micrograph digitally enhanced in b) and analyzed for domain direction in c) [5].

involves taking two misoriented images and digitally processing them together to find both

direction and magnitude of the domains seen. Digital techniques for image processing have also made it simpler to remove artifacts from surface imperfections and enhance contrast in micrographs that are often based on rotations

of less than twenty minutes of arc. An

example of a Kerr micrograph and

subsequent digital enhancements are shown

in Fig. 2. Kerr microscopy has advantages of

large range of possible magnifications,

speedy imaging, and, soon, quantification,

but sample preparation time is long,

equipment complicated and difficult, and resolution relatively limited. Other imaging

techniques include modifications on or use of electron scattering, transmission electron

microscopy (Lorentz microscopy), the Faraday effect on transmitted polarized light, X-rays,

and neutron scattering [5], but all have severe limitations or require extensive sample

preparation. An example of Lorentz microscopy, often used due to the unmatched resolution

of TEM, is shown in Fig. 3.

One of the more useful new tools in the study of magnetic domain structure has been the magnetic force microscope, or MFM. Generally, an MFM involves a magnetically coated stylus that is

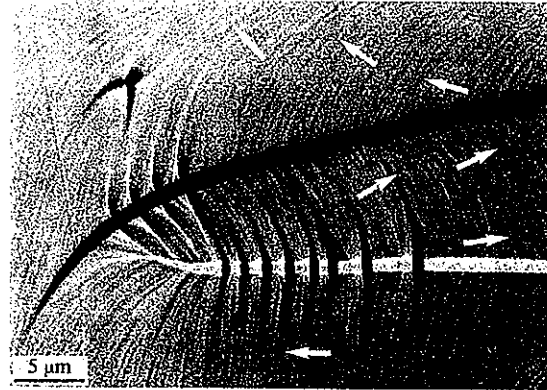


Fig. 3: A Lorentz micrograph permalloy showing "ripple" texture perpendicular to the average domain magnetization [5].

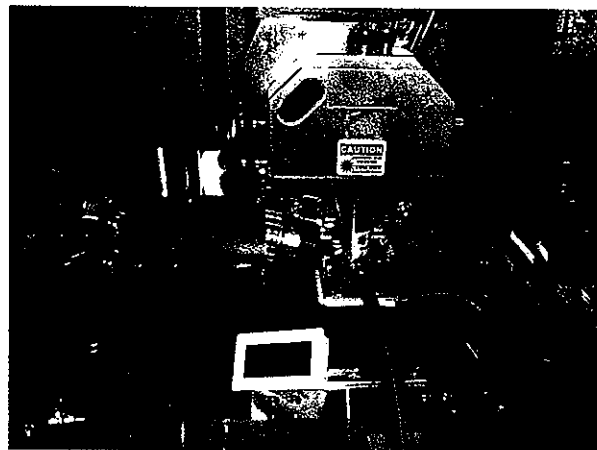


Fig. 4: Photo of an AFM/MFM head and assembly

dragged or tapped across the surface of a solid sample, with the surface stray field gradient causing a force on the tip and providing the contrast. The first such device was designed by Martin and Wickramasinghe at IBM and rastered a magnetic filament across an area of a sample to generate an image, with a resolution of about 100 nm [6]. Current devices, such as the Dimension 3100 AFM/MFM shown in Fig. 4, obtain topographical information by scanning the surface in a fashion similar to atomic force microscopy, then raising the tip a set

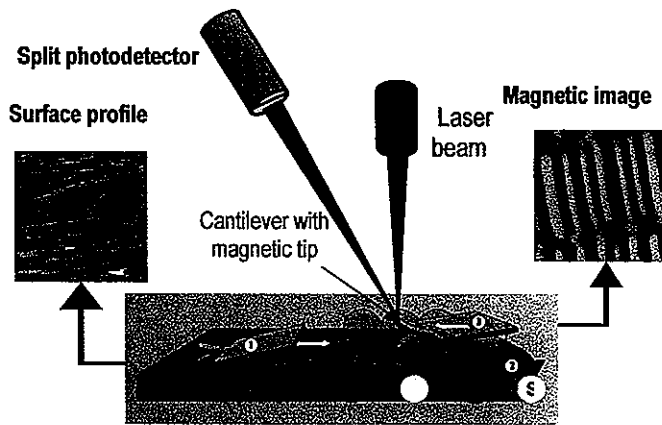


Fig. 5: Sketch representation of creating a magnetic force microscopy image.

height above the surface and rescanning. Thus the topology of the sample can be subtracted from the magnetic image and relatively rough sample surfaces can be tolerated [7]. A sketch representation of this process is shown in Fig. 5. Included

are the basic components of the device, including a laser and split photodetector to determine the z -deflection of the tip and, correspondingly, the surface. It should be noted that this strategy does not allow imaging of domains with field gradients oriented in the horizontal sample plane, and that the force on a magnetically coated tip providing contrast is from the vertical component of the stray field gradient (∇H). This makes domain imaging of thin films, where the preponderance of domains are often in plane due to shape anisotropy, more difficult, and in general analysis of any domain imagery slightly more complicated. However, the end result is much the same as that of scanning electron microscopy topographical imaging (where the contrast is also dependent on a gradient) without the disadvantage of a spatially limited detector. Unfortunately, one problem with using ultra-

sharp stylus tips coated with thin films is the irreproducibility of film thickness and accompanying irreproducibility of contrast from tip to tip. Thus, as long as quantitative measurements of the contrast are not desired, images obtained using this technique will both spatially and qualitatively match the physical picture of the sample domains and can be used by the researchers accordingly to interpret results of measurements in terms of domain structures.

The imaging possibilities of this new instrument were quickly realized. The spatial resolution easily reached the tens of nanometers scale even with rough samples. Some quite striking images have been taken over the last few years, including those shown here in Figures 6-8 [7]. As can easily be seen, many domain features that would have required complicated electron or Kerr microscopy techniques to image can be obtained in little time and with less difficult analysis. In fact, the open nature of the stage makes it possible to add new capabilities to the instrument, such as applied field, temperature control, or other needed capabilities.



Fig. 6: MFM image of a terfenol fracture surface. 75 μm scan by D. G. Lord. [7]

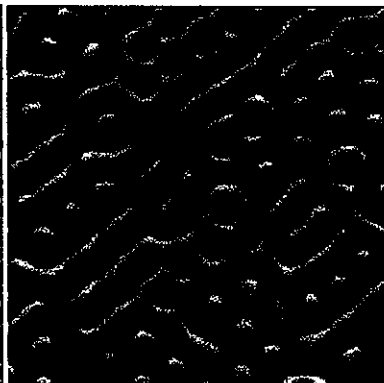


Fig. 7: Magnetic bubbles and stripes in an 8 μm thick garnet film. 100 μm scan by R. M. Westervelt.[7]

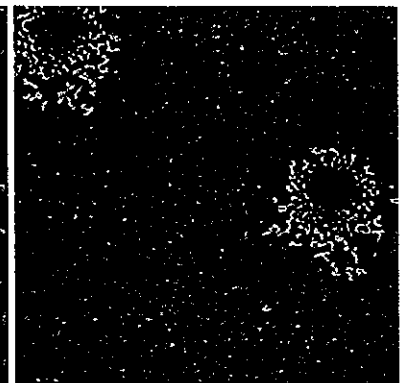


Fig. 8: MFM image of domains spreading from small regions of a Co/Pt multilayer that have low anisotropy compared to the rest of the film. 10 μm scan by L. Folks. [7]

2. CASE STUDIES: INTRODUCTIONS AND EXPERIMENTAL METHODS

Due to the varied nature of domain structures, as demonstrated in the previous section, it was not expected that one experiment or set of similar samples would provide enough information to draw broad conclusions. Even among the same material, geometry, coercivity, exchange, anisotropy, temperature, and geometry can significantly affect domain observations. Five different case studies, therefore, have been investigated, discussed, and compared in an attempt to discover trends and consistent patterns, with the end goal of clarifying relationships between domain structures and other magnetic measurements.

2.1 CASE STUDY 1: Stress in an FeSiAl thin film resulting in stripe domains

As-deposited FeSiAl films sputtered in Ar usually have high coercivity, low permeability and large out-of-plane magnetic anisotropy [8]. However, in hard disk drive read heads where they are used for shielding (see Fig. 9), their desired properties are exactly the opposite and are usually achieved by a post-deposition anneal [9, 10]. The drawback to this anneal is its relatively high temperature of $\sim 450^{\circ}\text{C}$, which is well above the temperature suitable for annealing of the entire read head assembly. The necessity to separate the process results in a degradation of the overall performance of the device. A deposition process providing desired soft magnetic properties in FeSiAl without annealing is therefore desirable, and investigations to this purpose discovered that nitrogen additions to the sputtering gas significantly affected film microstructure and magnetic properties in a way that can be useful for this application [11].

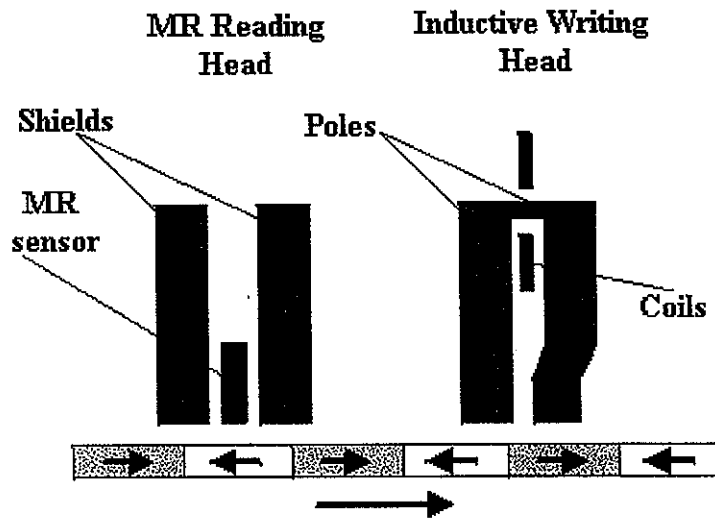


Fig. 9: Diagram of magnetic data, with a read/write head and parallel recording medium.

Several FeSiAl(N) films of varying N_2 partial pressure were deposited using radio frequency diode sputtering. An alloy target of Sendust composition (85 wt.% Fe, 10% Si, and 5% Al) was used to deposit films on (100) Si wafers with 300 nm thermally grown SiO_2 . A constant forward power of 1.43 W/cm^2 , fixed deposition time, and fixed combined pressure of Ar and N_2 gases were used to produce $1.7 \mu\text{m}$ films. The partial pressure of N_2 was set to values of 0, 1%, 2%, 3%, 4%, 5%, and 10%. Characterization of the films included vibrating sample magnetometry (VSM), TEM and SEM microstructural and compositional analysis, stress analysis, and magnetic force microscopy. Stress analysis was accomplished by measuring the curvature of long strips on an atomic force microscope, using the compensated z position of the tip at contact and subtracting from the center to determine deflection. Equation (1) describes the stress in terms of the deflection, lateral position, substrate and film thicknesses, film and substrate moduli, and Poisson's ratio of the substrate, and Fig. 10 illustrates the bowing of the substrate due to the film deposition.

$$\sigma = \frac{yE_s D^2}{3x^2 t(1-\rho_s)} \left(1 - \frac{E_f t}{E_s D} \right) \quad (1)$$

In equation (1), y is the deflection, x is the lateral position, D is the substrate thickness, t is the film thickness, E_s is the Young's modulus of the substrate, E_f is the Young's modulus of the film, and ρ_s is the Poisson's ratio of the substrate.

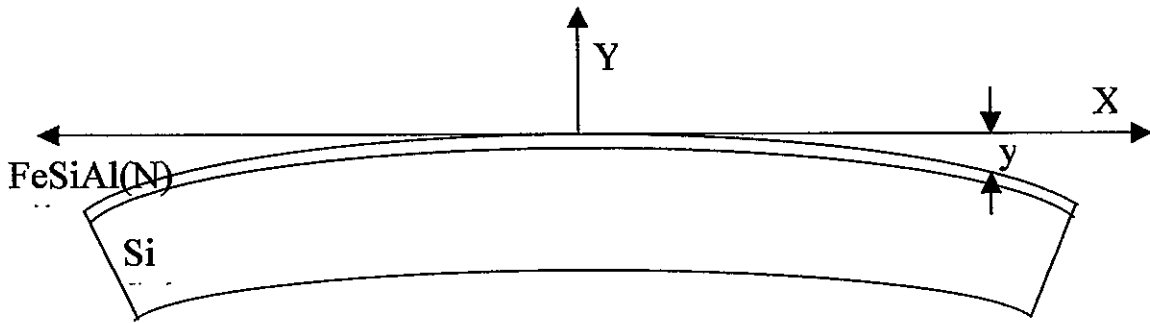


Fig. 10: Diagram of substrate bowing under stress from film deposition.

For the *in-situ* applied field measurements, an electromagnet capable of producing an in-plane field up to about 56 kA/m (700 Oe) was mounted on the sample stage.

Demagnetization of the samples was accomplished by applying an ac field with decaying amplitude along the desired applied field direction.

2.2 CASE STUDY 2: Magnetization reversal in CoFeHfO films

CoFeHfO films have received considerable attention because of their combination of soft magnetic properties and high-frequency characteristics. It has been reported that CoFeHfO films deposited by reactive sputtering under a dc magnetic field typically have an M_S value exceeding 1T, a coercivity of a few hundred A/m and a high electrical resistivity of the order of magnitude of $600\mu\Omega\text{m}$ [12]. These films were found to contain Fe (or Co-Fe) rich bcc

nanograins and an amorphous matrix containing a large amount of Hf and O [12]. The matrix provides a low conductivity barrier to the long range conduction of current, allowing for very high frequency performance due to suppressed eddy current loss, while the nanograins allow for a relatively high permeability of around 150 along the hard axis. The low loss factor of these films remains constant up to hundreds of megahertz, making CoFeHfO films a promising candidate for high frequency device applications.

A CoFeHfO film (800 nm thick) and a CoFeHfO (10 nm) film overcoated with CrSi (10 nm) were used in this study. The CoFeHfO layers of the samples were deposited by reactive rf-sputtering using an Ar + O₂ atmosphere onto Si (100) substrates with 200 nm of surface SiN. These films were annealed at 250°C for one hour in a magnetic field to induce an in-plane uniaxial anisotropy. Magnetization curves were measured from 7mm by 7mm samples using VSM along both the easy and hard axes of magnetization. Studies of the domain structure and magnetization reversals were made using MFM with tips magnetized perpendicular to the sample plane and the electromagnetic stage described above. Two series of MFM images were taken from each sample under various fields (up to 43.8 kA/m) applied *in-situ* along the easy and hard axes of magnetization of the films.

2.3 CASE STUDY 3: Anisotropy in a Complex Magnetic Material

Gd₅(Si_xGe_{1-x})₄ has recently received much interest due to its extraordinary response in several magnetic and electronic properties during changes in temperature and magnetic field. These include colossal magnetostriction, giant magnetoresistance, and giant magnetocaloric effect. Gd₅(Si_xGe_{1-x})₄ undergoes a magnetic-crystallographic transformation at a Curie

temperature which varies from ~40 K to 320 K dependent on the Si to Ge ratio. During the transformation the material exhibits changes in strain as high as 10^4 parts per million, magnetoresistance of about 25%, and the largest magnetocaloric effect (an adiabatic temperature change when magnetized) to date

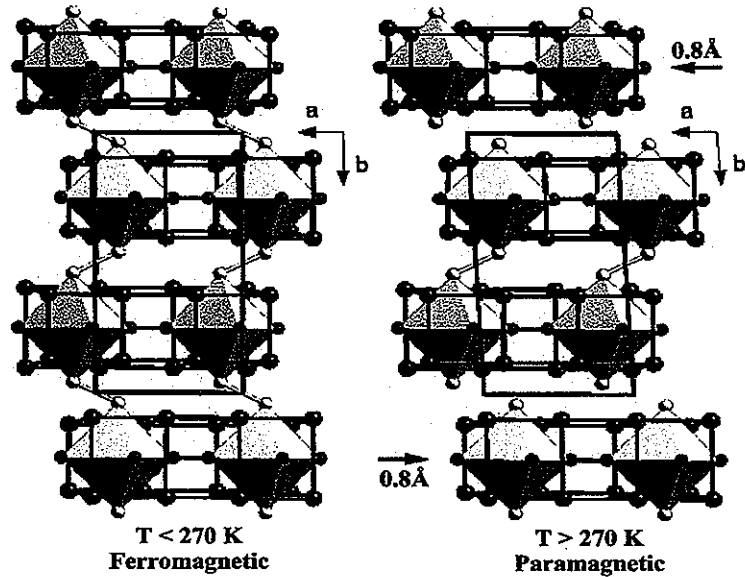


Fig. 11: Crystal structure of $Gd_5(Si_xGe_{1-x})_4$ in both low temperature and high temperature phases. Blue atoms are Gd atoms and red and yellow are Si and Ge, which are often interchangeable.

[13]. The phase transition is a magnetic-martensitic transformation from a paramagnetic-monoclinic crystal structure at higher temperatures to a ferromagnetic-orthorhombic crystal structure at lower temperatures and involves shear of sub-nanometer atomic layers in a complex crystal lattice through reversible breaking and reforming of covalent Si(Ge)—Si(Ge) bonds between the layers [13]. A diagram of the crystal structure can be seen in Fig. 11.

Since initially the magnetic structure of this material was unknown, the assumption had been that the magnetic moments on the Gd atoms in the ferromagnetic state were nearly perpendicular to the b -axis, akin to magnetic structures observed in related Tb_5Si_4 and Tb_5Ge_4 compounds. However, exploratory single crystal MFM measurements indicated

differently, so more comprehensive characterization was initiated, including temperature dependent VSM and MFM.

VSM measurements were collected using a $\text{Gd}_5(\text{Si}_2\text{Ge}_2)$ single crystal cube with all three axes identified using x-ray diffractometry. The sample temperature was maintained below the Curie point/transition temperature using a dry ice/ethanol mixture and hysteresis loops measured along the three principal axes of the crystal using a magnetizing field of maximum amplitude of 600 kA/m. Anisotropy coefficients were calculated from the hysteresis loops.

An *in situ* MFM study of the phase transformation was carried out using an atomic/magnetic force microscope equipped with a sample heating/cooling stage. The sample stage consisted of a thermoelectric cooling unit capable of varying the sample temperature from about -30°C to $+50^\circ\text{C}$, a copper transfer plate for better temperature uniformity, and a semi-enclosed chamber filled with flowing dry Argon gas to prevent condensation of water vapor at low temperatures. Each $\text{Gd}_5(\text{Si}_2\text{Ge}_2)$ sample was attached to the stage using thermal tape to ensure good thermal contact. Temperature was monitored and maintained within ± 0.2 K using a thermocouple attached to the heating/cooling stage. Each single crystal image was obtained from a different sample cut by electric discharge machining (EDM) with the specified crystal axis oriented normal to the largest sample face.

A high-purity polycrystalline sample of composition $\text{Gd}_5(\text{Si}_{2.09}\text{Ge}_{1.91})$ was also cut and polished for comparison with the single crystal samples. The domain structures during the phase transition of this sample were recorded on the same heating/cooling stage.

Single crystal transition temperatures were measured by slowly increasing and decreasing the temperature of the sample at a rate of less than 0.017 K/s while imaging the sample with both AFM and MFM. The transition temperature was recorded as the temperature at which the sample surface shifted due to the martensitic nature of the transition and magnetic contrast either appeared or disappeared, depending on transition direction. For the polycrystalline sample, the transition was recorded as the temperature at which the magnetic image began or finished changing.

2.4 CASE STUDY 4: Melt-spun Fe₇₅Si₁₀B₁₅ Ribbons

Fe-rich transition-metal type amorphous alloys with high boron content have been reported to have good soft magnetic properties as shown by static magnetic measurement [14]. Thus, an amorphous ribbon should provide good in-plane shape anisotropy and show significant changes in domain structure with changes in shape or stress.

As an exploratory experiment, therefore, Fe₇₅Si₁₀B₁₅ ribbons were melt spun and mechanically deformed in the center to produce a gradient of physical distortion through the ribbon. Two bent ribbons were then mounted for microscopy to allow for traversing the surface while maintaining a parallel plane with the surface necessary for imaging.

2.5 CASE STUDY 5: Magnetic Tunnel Junction Behavior

Magnetic tunnel junction behavior, first observed at room temperature by Moodera and co-workers [15], is a topic of great current scientific and technological interest. The electric

current through a magnetic tunnel junction relies on spin-dependent tunneling of the electrons from a ferromagnetic layer, through an insulating barrier, into another ferromagnetic layer, with the electronic spins correlated by ferromagnetic exchange forces within the magnetic domains in the ferromagnetic layers [16]. Tunnel junctions and their switching have been imaged using magnetic microscopy [17], but the true magnetic domain behavior of a spin-dependent tunnel junction as it reverses from high resistance to low resistance, and vice versa, has never before been observed while the resistance is simultaneously being measured.

The resistance of a magnetic junction depends on the relative magnetization directions in the two ferromagnetic electrodes. Together with the electron band structure – in particular the differences in the relative densities of states in the majority “spin up” half band and the minority “spin down” half band as shown in Fig. 12 [18] – the resistance of the junction will vary significantly, depending on the applied field. Parallel alignment of the magnetization in the two ferromagnetic electrodes allows the conduction electrons that tunnel through the insulating barrier layer to find a similar density of states on the other side. Conversely, antiparallel alignment of magnetic domains in the two electrodes leads to majority conduction electrons from a high density of states finding that the density of states is much lower on the other side. This results in a higher resistance in the antiparallel configuration than in the parallel configuration.

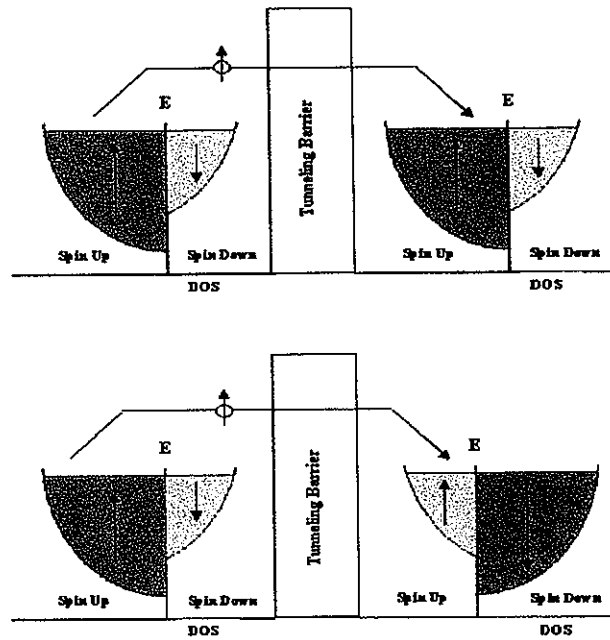


Fig. 12: Schematic of band structures in a magnetic tunnel junction showing the majority spin up and minority spin down half bands, and how the resistance is affected by the orientation of the magnetization in the electrodes on either side of the tunneling barrier [5]

Multilayers of the structure Si(substrate)-NiFe(12nm)-AlO_x(1.5nm)-FeCo(5.4nm)-CrPtMn(32.8nm)-Al(5.4nm) were fabricated into magnetic tunnel junctions by Non-Volatile Electronics, Inc. [19], as sketched in Fig. 13. The junctions of interest had a tapered ellipsoidal shape, with the full junction multilayer stack structure covering half the ellipsoidal

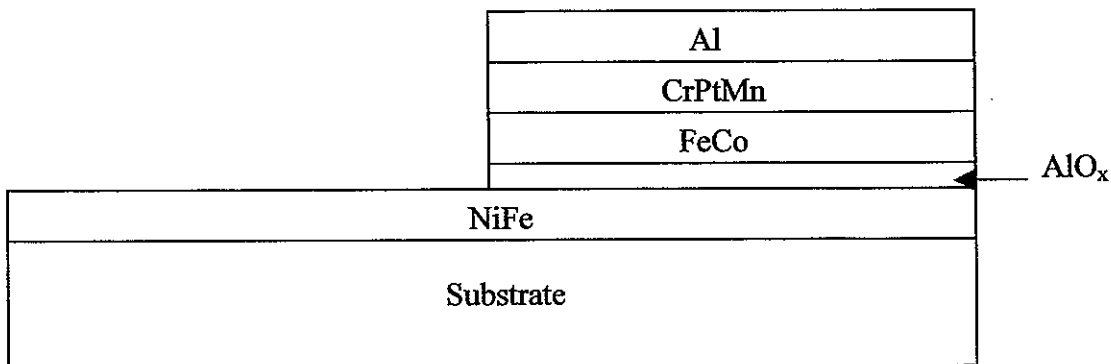


Fig. 13: Schematic of magnetic tunnel junction sample.

area, and the other half the exposed NiFe free layer (divided along the long axis). Enough area of the stack and free layer were exposed from beneath Al interconnects to allow imaging by MFM. Easy axes were induced perpendicular to the ellipsoid axis by annealing under an applied magnetic field. One such multilayer device, as shown in Fig. 14, was selected and connected to a circuit via wire-bonding. The tapered half-ellipsoidal shape of this junction had dimensions of $\sim 12\mu\text{m}$ at the widest point along the short axis and $\sim 40\mu\text{m}$ along the long axis. This device was then imaged on an MFM stage modified to include *in-situ* applied field capability.

During imaging, a potential of 50mV was applied across the magnetic tunnel junction. The stack was positioned in the right half of the image and the free layer in the left half for easy comparison of the junction multilayer stack to the free layer electrode. The tip of the ellipsoid from which domain nucleation began was positioned at the top of the images. As the free layer of the junction was known to have a coercivity of

$\sim 800\text{A/m}$ (10 Oe), the field was first increased to $+2.4\text{KA/m}$, decreased to -3.6KA/m , and returned to $+2.4\text{KA/m}$, with domain images taken by MFM at intervals of typically 400 A/m. Images were taken at smaller field intervals in the hysteretic region, where changes in domain structure with changing field were much more rapid, and resistances were recorded using a Keithley 3000 series sourcemeter at all field steps.

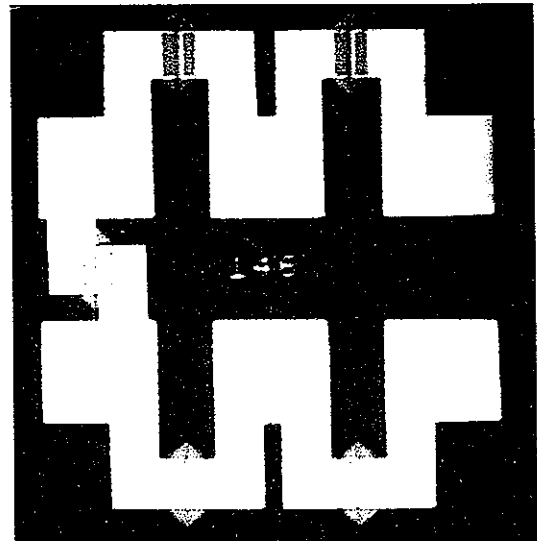


Fig. 14: Optical micrograph of NVE tunnel junction test pattern, with ellipsoid junctions visible. Magnification 250X.

3. RESULTS

3.1 CASE STUDY 1: Stress in an FeSiAl thin film resulting in stripe domains

Initial vibrating sample magnetometry measurements are summarized in figures 15, 16, and 17, with the film stresses included in figures 16 and 17.

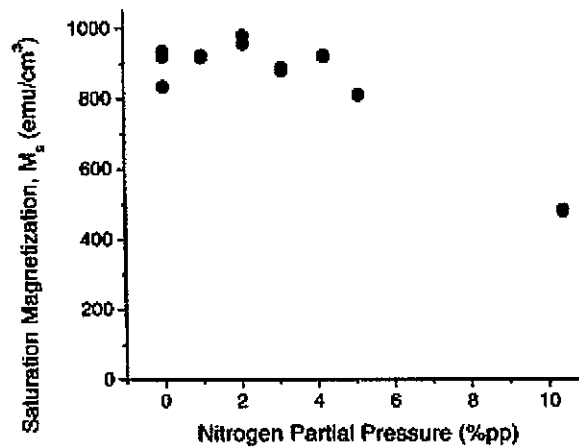


Fig. 15: Saturation magnetization as a function of N partial pressure.

There is quite a drastic transition in properties from the 4ppN₂ film to the 5ppN₂ film evident in the stress, coercivity, and saturation field curves. Although this change is not as visible in the M_s data, the microstructural information obtained via SEM and TEM microscopy (Fig. 18) confirms a significant microstructural change in the films between those fabricated at these partial pressures of nitrogen.

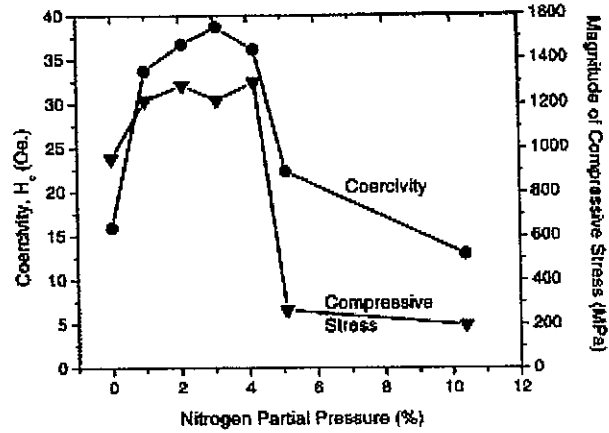


Fig. 16: In-plane coercivity (H_c) and magnitude of compressive stress as functions of N partial pressure.

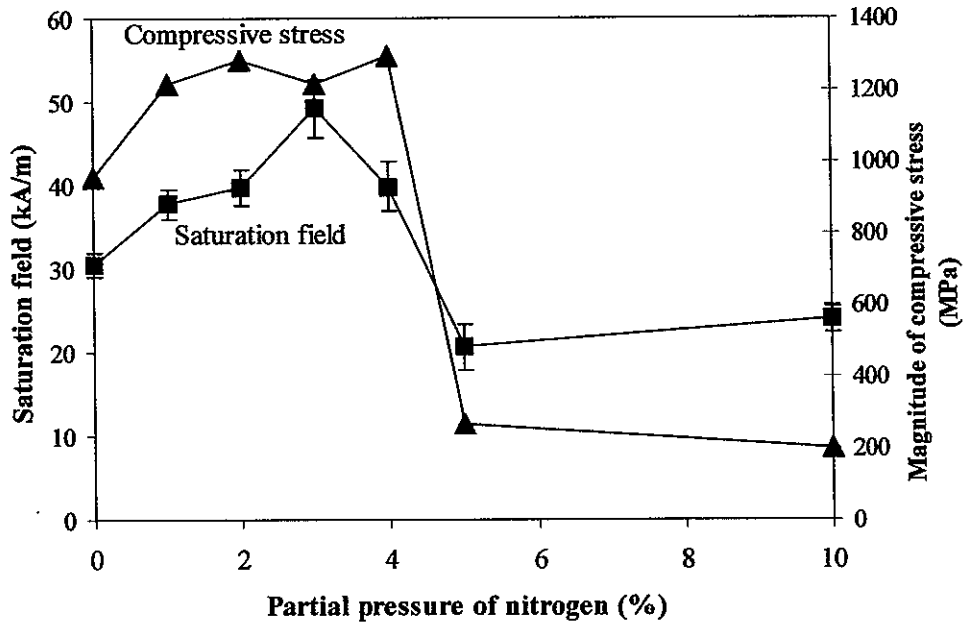


Fig. 17: Film saturation field and compressive stress as a function of partial pressure of N.

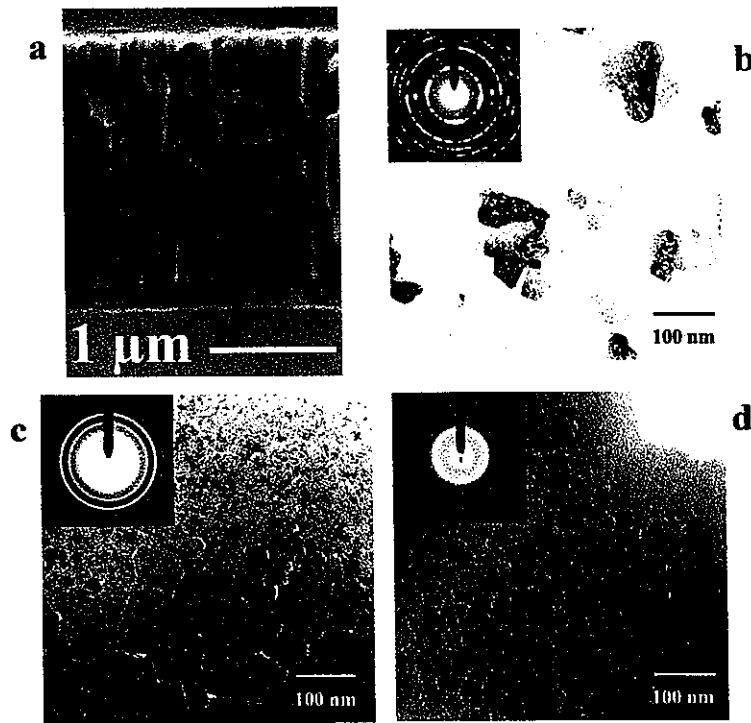


Fig. 18: SEM (a) and TEM (b-d) micrographs of 0ppN₂ (a and b), 5ppN₂ (c) and 10ppN₂ (d). Electron diffraction patterns are included for the TEM micrographs.

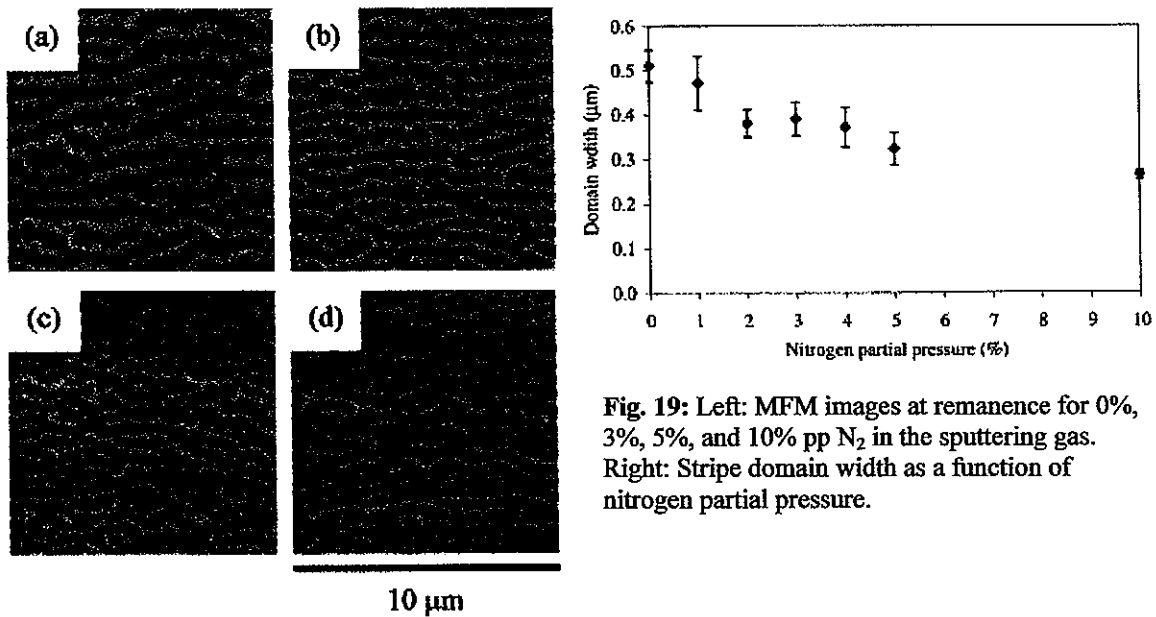


Fig. 19: Left: MFM images at remanence for 0%, 3%, 5%, and 10% pp N₂ in the sputtering gas. Right: Stripe domain width as a function of nitrogen partial pressure.

MFM results, then, were expected to show some change between the same samples. Fig. 19 shows both qualitative and quantitative differences between the domain structures at remanence. If the domain width plot is examined, it appears that there is simply an incremental change across the entire composition range. This observation is supported by the remanence images, which show both a continual decrease in domain width and apparent long range length (the lines of the stripes are less straight). However, *in-situ* applied field imagery from film to film is quite different; as can be seen in figures 20-22, the high field nucleation of domains for the higher pp N₂ samples is much more random (there is less domain pinning) and domain rotation finishes at much lower fields, corresponding to the smaller saturation fields measured in the VSM. These figures include the VSM hysteresis loops for each sample.

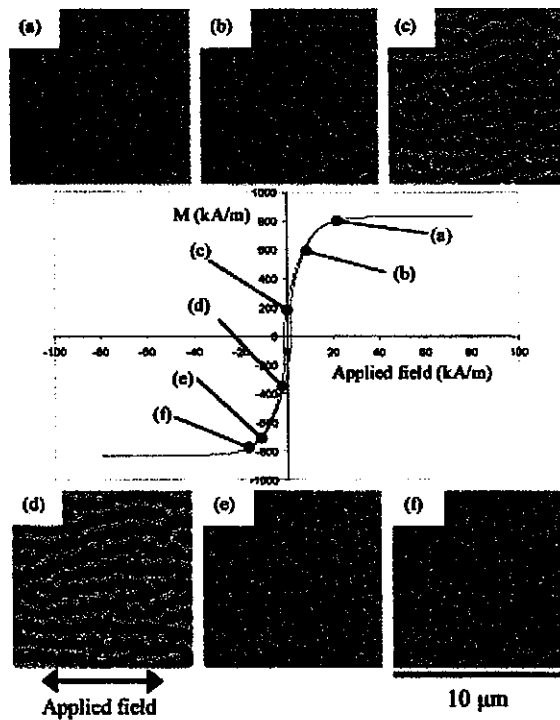


Fig. 20. MFM images obtained from the 0% pp N film in applied fields of (a) 19.9 kA/m, (b) 8.0 kA/m, (c) 0 kA/m, (d) -5.5 kA/m, (e) -15.9 kA/m, and (f) -20.0 kA/m

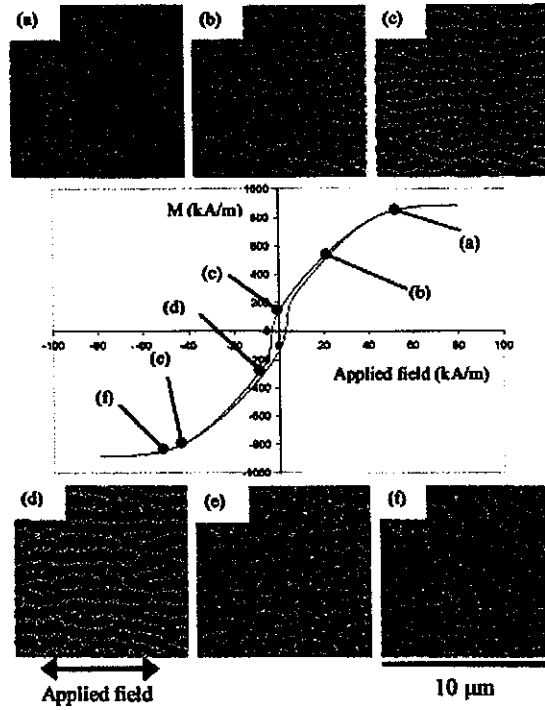


Fig. 21. MFM images obtained from the 3% pp N film in applied fields of (a) 51.8 kA/m, (b) 19.9 kA/m, (c) 0 kA/m, (d) -8.0 kA/m, (e) -43.8 kA/m, and (f) -51.8 kA/m

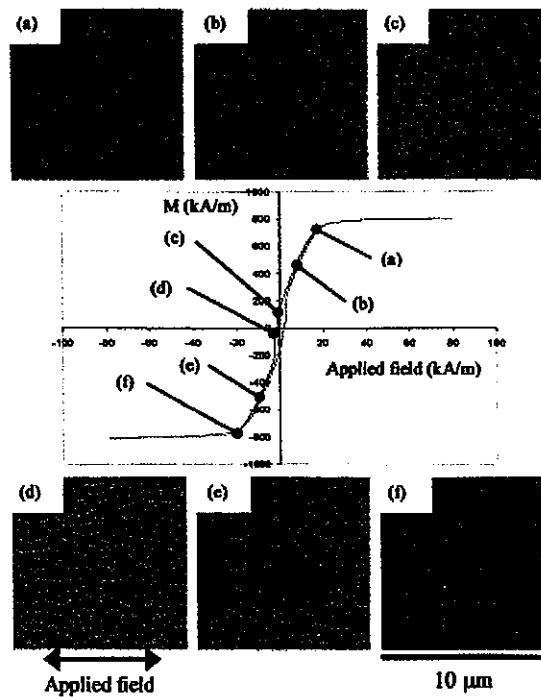


Fig. 22. MFM images obtained from the 5% pp N film in applied fields of (a) 19.9 kA/m, (b) 9.6 kA/m, (c) 0 kA/m, (d) -2.4 kA/m, (e) -10.0 kA/m, and (f) -19.9 kA/m

In fact, the pinning of domains despite saturation of the sample is the greatest difference seen from film to film, and is illustrated in Fig. 23. This figure shows the 0% and 5% pp N₂ films at remanence after being magnetized to saturation in opposite directions. While the 5% film shows little similarity between the two images, the 0% film demonstrates several areas that are clearly domains with complementary contrast. In effect, the domain walls have been pinned to the same location despite the apparent saturation and destruction of stripes at higher fields.

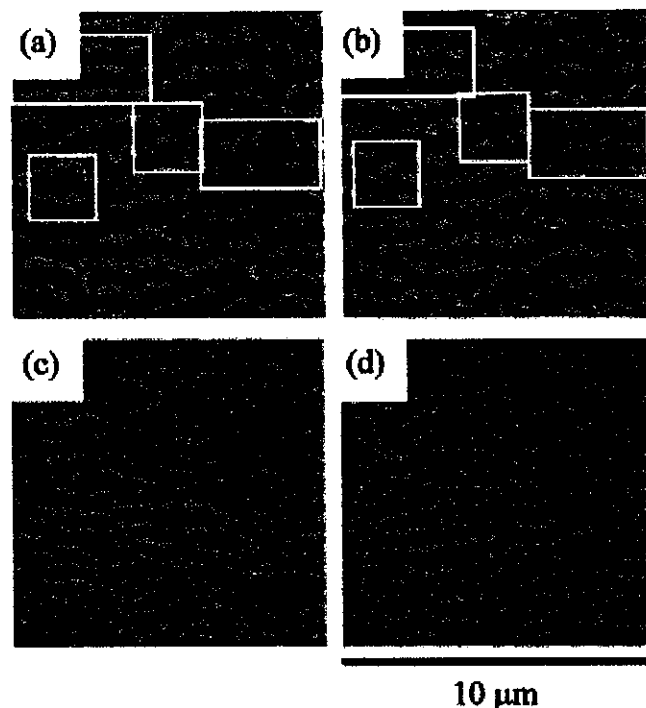


Fig. 23: MFM images obtained from the 0%pp N film at the oppositely magnetized remanent states are shown in (a) and (b). Notice the complementary contrast of the highlighted regions. The MFM images in (c) and (d) were obtained from the 5%pp N film at the oppositely magnetized remanent states

3.2 CASE STUDY 2: Magnetization reversal in CoFeHfO films

The magnetization curves along the easy and hard axes of the samples are shown in Fig. 25-26. The observed reduction in magnetization at high field in the thin CoFeHfO film (Fig. 24b) is likely due to the diamagnetic response of the Si substrate which was not subtracted

from the measured signal. The hysteresis loop parameters are summarized in Table I. The easy-axis hysteresis loops of both the thick CoFeHfO film and the thin film exhibit high squareness, suggesting that the magnetization reversal involves mostly irreversible domain

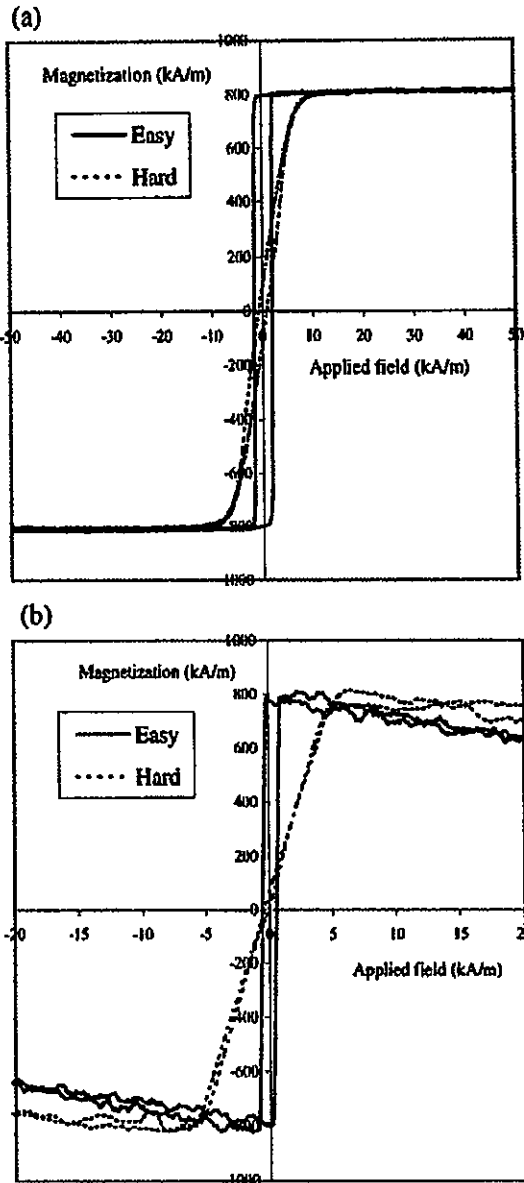


Fig. 24: Hysteresis loops measured along the easy and hard directions. (a) CoFeHfO (800 nm) film, (b) CrSi/CoFeHfO (10 nm) film.

wall motion in the films. The hard-axis loops of both films indicate domain rotation. The anisotropy fields were measured to be 6.0 kA/m and 5.4 kA/m for the thick and thin films, respectively.

Both films showed significant changes near their coercive fields when a field was applied along their easy directions. Fig. 25 gives examples of MFM images of the thinner film under various fields applied along the easy axis. The domain pattern remained essentially the same when the reversed field was below the coercive field. As the reversed field was increased to about the coercive field (670 A/m), large-

scale changes in the domain pattern were observed, accompanied by a local switching of

image contrast in regions about $0.2 \mu\text{m}$ in size. The domain structure remained unchanged as the reversed field was further increased. Similarly, the thick CoFeHfO film exhibited greatest changes in domain structure when the reversed field was increased from about 2 kA/m to 3 kA/m, which was close to the coercivity.

TABLE I
MAGNETIC PROPERTIES OF THE THICK CoFeHfO (800 nm) SAMPLE AND
THE THIN CoFeHfO (10 nm) SAMPLE ALONG THE EASY AND HARD
AXES OF MAGNETIZATION

CoFeHfO film (thickness: 800 nm)			
	Coercivity (A/m)	Remanent magnetization (kA/m)	Susceptibility at coercive point
Easy axis	1777	794	2448
Hard axis	765	101	125
CrSi-coated CoFeHfO film (thickness: 10 nm)			
	Coercivity (A/m)	Remanent magnetization (kA/m)	Susceptibility at coercive point
Easy axis	670	785	2033
Hard axis	< 361	< 25	149

When a field was applied along the hard axis of the thin CoFeHfO film, a distinctive reversal process was observed, as shown in Fig. 26. A domain pattern (width $< 0.5 \mu\text{m}$) with out-of-plane stray field components became apparent at about 1.3 kA/m. As the applied field was increased, the domain features rotated gradually. During this process, the image contrast *increased*, reached a maximum when the striations aligned perpendicular to the field (i.e., parallel to the easy axis) and then diminished as the sample approached saturation. This is in contrast to the results obtained from the thick CoFeHfO film that showed relatively little domain switching and a smaller change in contrast.

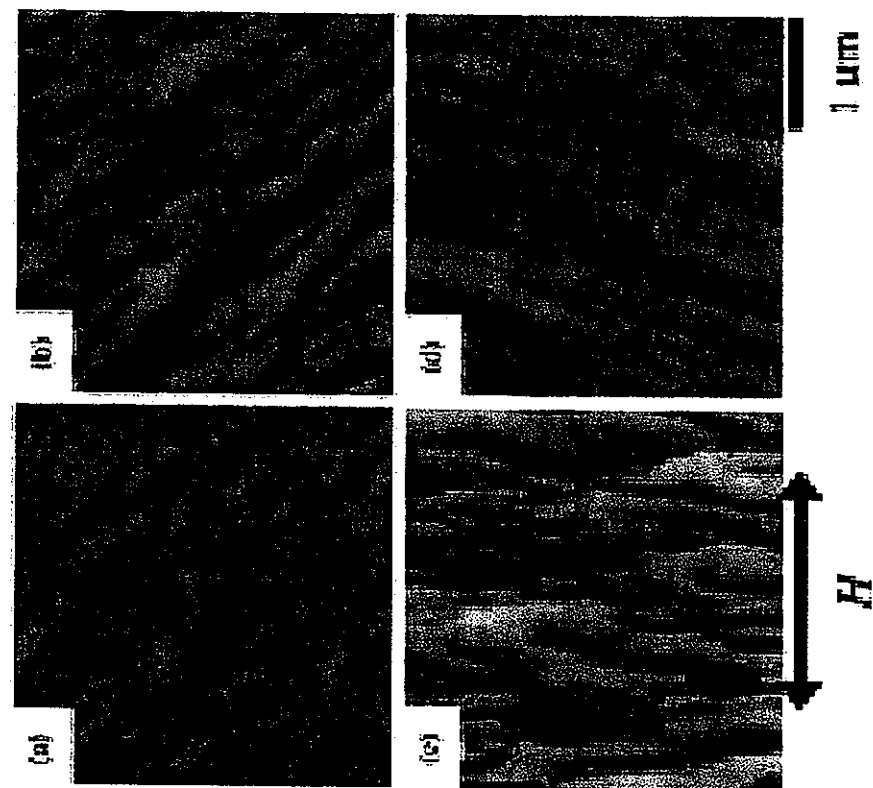


Fig. 25: MFM images obtained from the 10 nm thick CoFeHfO film under magnetic fields of (a) 0 A/m, (b) 398 A/m, (c) 1.59 K A/m and (d) 2.47 K A/m applied along the easy axis. The easy axis coercivity is 670 A/m.

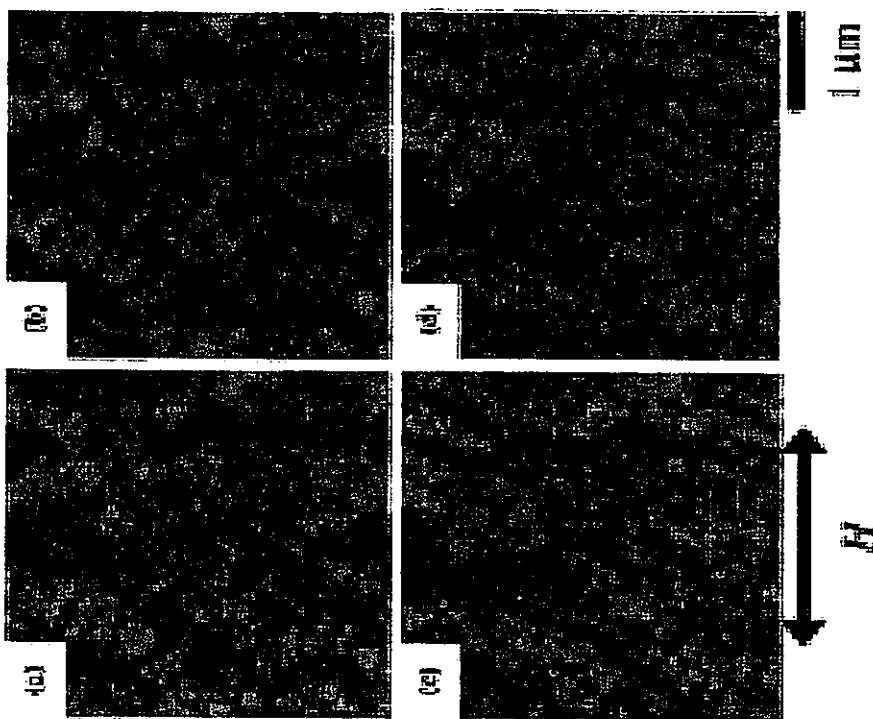


Fig. 26: MFM images obtained from the 10 nm thick CoFeHfO film under magnetic fields of (a) 799 A/m, (b) 2.39 K A/m, (c) 6.45 K A/m and (d) 9.95 K A/m applied along the hard axis.

3.3 CASE STUDY 3: Anisotropy in a Complex Magnetic Material

Fig. 27 shows the domain structure of three different $\text{Gd}_5(\text{Si}_{-2}\text{Ge}_{-2})$ single crystals in the ferromagnetic state, with the a, b, and c-axes perpendicular to the surface, respectively. It should be noted that each face was aligned at room temperature, so the a-axis image was slightly misaligned after a significant martensitic shift during the transition. The crystal with the c-axis perpendicular to the surface was known to change phases due to significant lateral movement of physical surface features ($\sim 15 \mu\text{m}$) at a likely transition temperature.

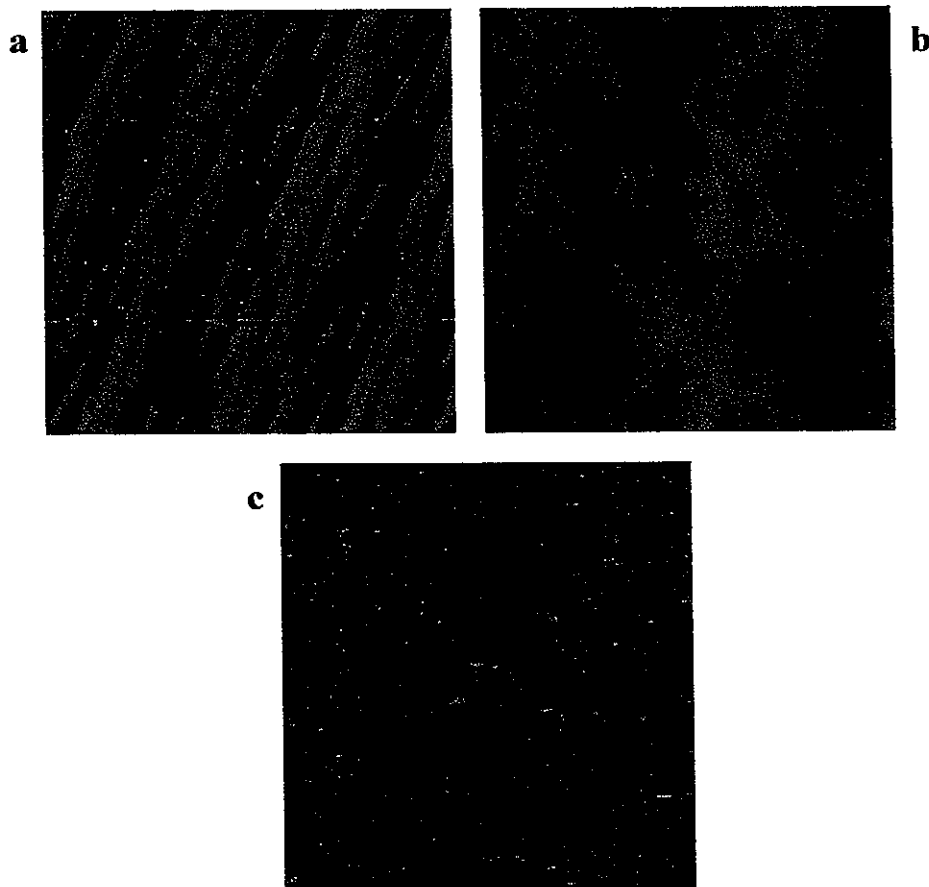


Fig. 27: 20x20 μm images of single crystals in ferromagnetic state (at 260K) with, from top left, a-, b-, and c-axes perpendicular to the surface.

The difference between the three axes is striking. The a-axis image exhibits stripes of relatively strong contrast and of periods of two lengths scales, the first on the scale of 1-2 μm and the second on the scale of $\sim 5\mu\text{m}$, the b-axis highly branched rosette domains, and the c-axis shows complete uniformity. The lack of contrast in the c-axis image was verified to well below the transition temperature and for multiple transition cycles, and in all cases the transition from paramagnetic to ferromagnetic or vice versa was very rapid – within a ΔT of less than 0.1 $^{\circ}\text{C}$ and a time of less than a few seconds. There was, however, a transition temperature hysteresis of $\sim 2^{\circ}\text{C}$ in all samples.

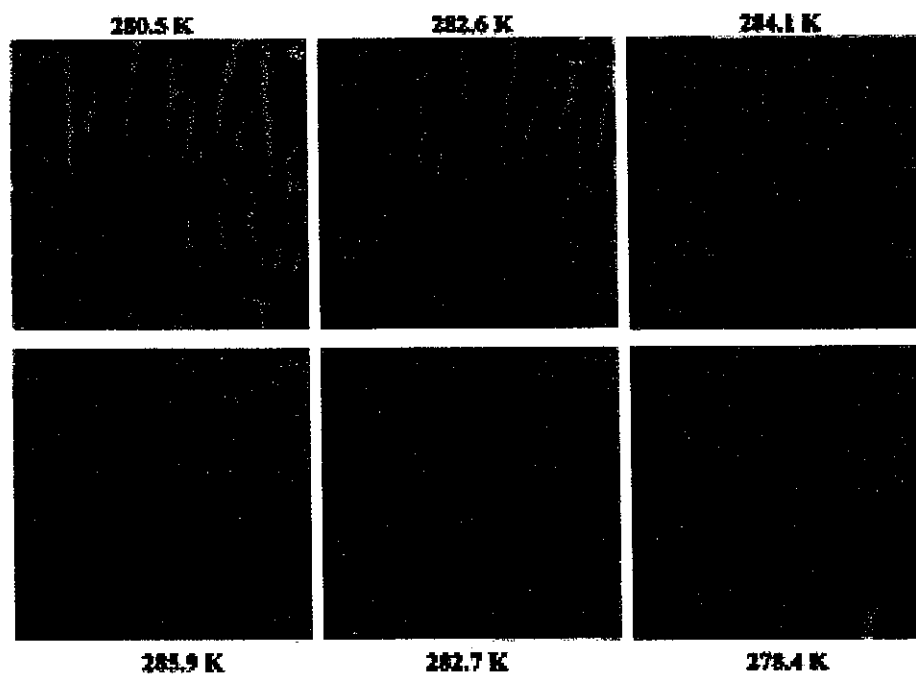


Fig. 28: MFM images showing the phase transition of polycrystalline $\text{Gd}_5(\text{Si}_{2.09}\text{Ge}_{1.91})$ sample (3 $^{\circ}$ phase contrast, 20 μm scans). The temperature of the sample is marked for each image.

The domain structures of the polycrystalline sample were, as expected, quite different. However, there was also a marked increase in the ΔT necessary for the phase transition to progress completely. Both of these observations are illustrated in Fig. 28.

The transition temperatures measured for all samples were in good agreement with thermal expansion data, allowing for the interpretation that domain structures in the single crystals were only present in the ferromagnetic phase [20]. Fig. 29 shows the a-axis sample in the paramagnetic and ferromagnetic states as an example.

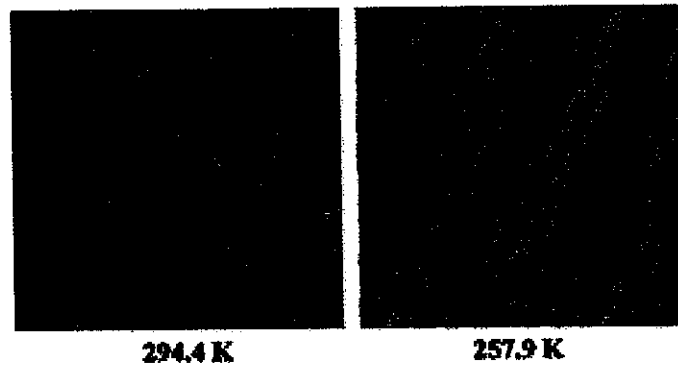


Fig. 29: a-axis single crystal $\text{Gd}_5(\text{Si}_2\text{Ge}_2)$ sample in paramagnetic and ferromagnetic states (left and right). Temperature of the sample is as marked.

Vibrating sample magnetometry data for the single crystal cube is shown in Fig. 30 and

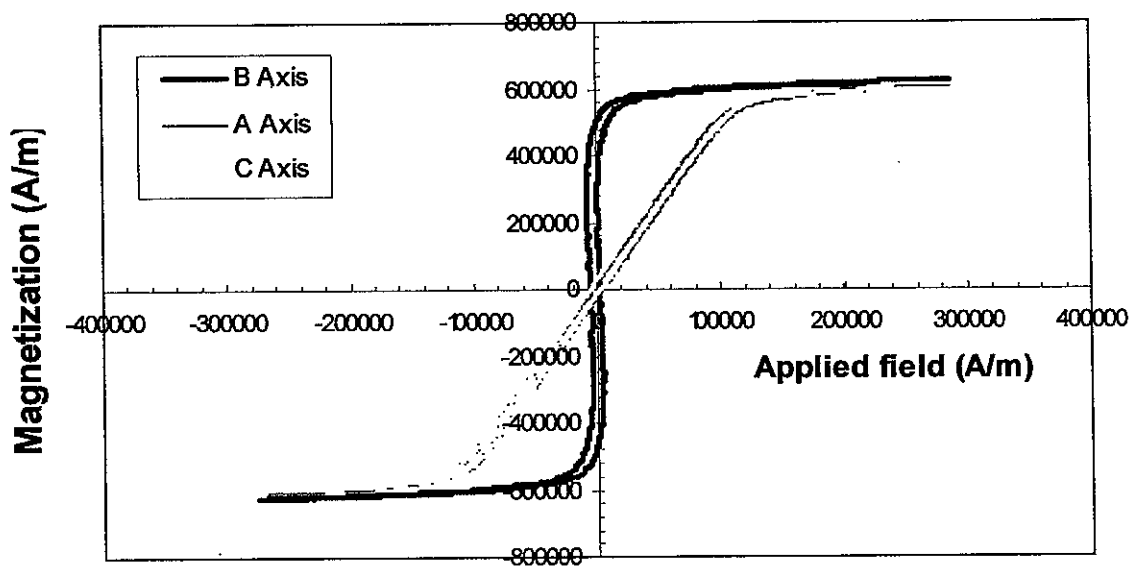


Fig. 30: VSM hysteresis loops for a-, b-, and c-axes of single crystal $\text{Gd}_5(\text{Si}_2\text{Ge}_2)$ at 260K.

indicates quite clearly a uniaxial anisotropy along the b-axis of the crystal, with the a- and c-axes being equally hard.

In order to perform the anisotropy calculations, it is assumed that the magnetization curve is reversible and that the magnetization mechanism along the hard axis is entirely by reversible moment rotation. The anisotropy energy is then the difference in energy required to saturate magnetization along the hard and easy directions. This assumption is not entirely valid, but is often used to make analysis practical. If the energy to saturate in each direction is the area between the magnetization curve and the M axis, then the anisotropy energy is the difference in these two areas [21]. To determine the anisotropy coefficients, parametric equations were fitted to each magnetization curve and linear equations fitted to the linear portions of the a- and c-axes. For uniaxial anisotropy, $E_a = K_1 \sin^2 \theta + \dots$ [21], so

$K_I = W_{[001]} - W_{[010]} = 4.1 \pm 0.2 \times 10^4 \text{ J/m}^3$. This value for K_I is comparable to iron and to uniaxial garnets, is an order of magnitude less than Co or $\text{BaFe}_{12}\text{O}_{19}$, and is an order of magnitude larger than nickel.

3.4 CASE STUDY 4: Melt-spun $\text{Fe}_{75}\text{Si}_{10}\text{B}_{15}$ Ribbons

Images shown in Fig. 31 and 32 were arranged as a collage of separate images, spatially oriented, with each image 40 μm square. Rectangular micrographs were merged from 40 μm square single images using photo editing software.

In both Figures 31 and 32, as the strain increases (toward the right in both figures), the magnetic contrast increases, the band width of the domains increases, and the structure

transforms qualitatively. In fact, in Fig. 31c, the far right of the image shows a transition to another domain structure entirely, as highlighted below.

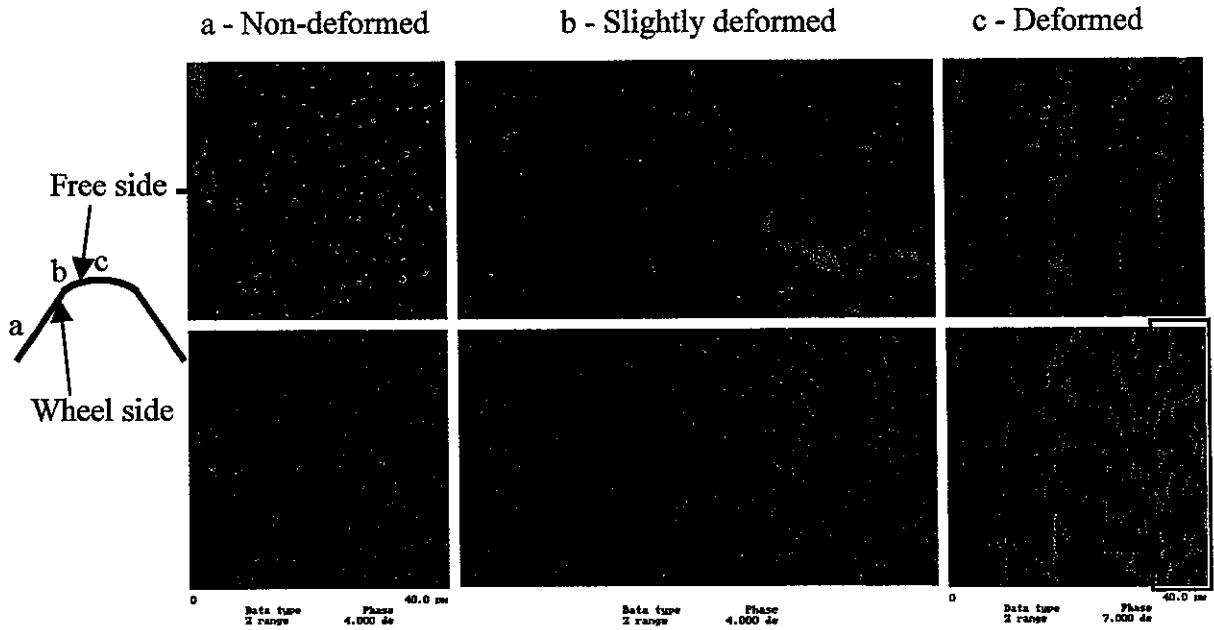


Fig. 31: Comparison of AFM topography (top) to MFM magnetic information (bottom). Slip planes can easily be seen in the surface, with increasing magnetic contrast and band width as the physical deformation increases.

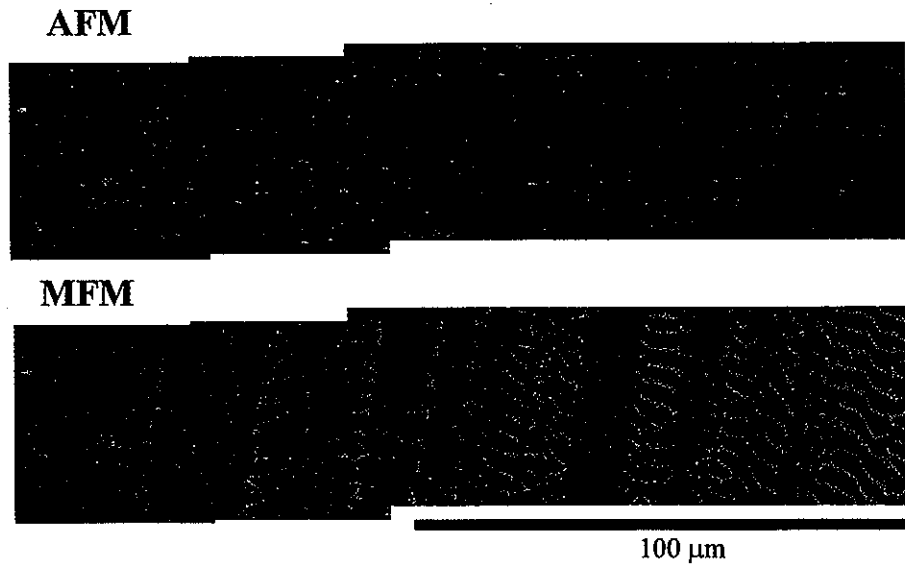


Fig. 32: Comparison of AFM topography (top) to MFM magnetic information (bottom), similar to Fig. 13 but in a different location on the ribbon.

In this area, the most highly deformed of any of the regions, the degree and length scale of domain branching is quite high over most of the surface, even in the areas that still show regular stripes. The highlighted area appears to show a shift from the dominant stripe structure towards complete branching without the regular stripe length scale period.

3.5 CASE STUDY 5: Magnetic Tunnel Junction Behavior

For all of the following images, the junction stack is located on the right side of the image (R) and the exposed free layer is the left (L), as shown in Fig. 33. The step boundary, which is the physical edge between the junction stack and the free layer, is seen as a straight line in the center of the magnetic image, with the separation allowing for easy comparison.

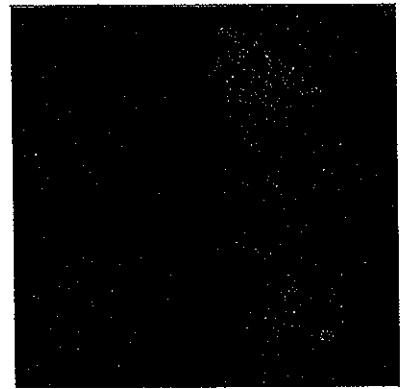


Fig. 33: Representative image of junction device.

The field-resistance hysteresis loop for the junction, representative images of increasingly negative field, and increasingly positive field are shown in Fig. 34 through 36, respectively. $\Delta R/R$ for this junction was $\sim 20\%$, indicating simply that the device was working and representative of a fairly basic tunnel junction. As expected, for applied fields well outside the hysteretic region of the R-H loop, the MFM images show no magnetic contrast on either the free layer side or the multilayer stack side of the junction. This is due to saturation of the magnetization in the device plane, leaving no perpendicular contrast to image. In the hysteretic region, domain structure becomes more complex, rotating significantly out of the sample plane. This smaller scale structure appears before the resistance begins to change.

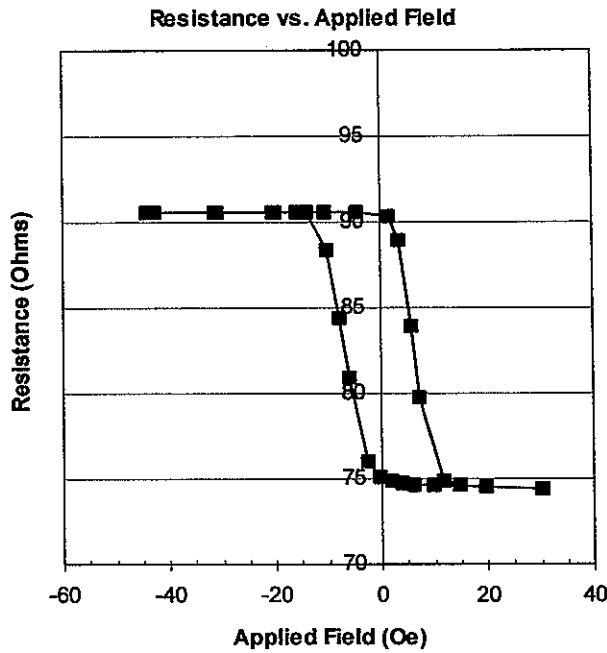


Fig. 34: Plot of junction resistance versus planar applied field.

domains nucleated in the junction at about 10 Oe in the loop of Fig. 34, and spread to the entire area through the transition and persist in the junction stack until the field strength reaches about -20 Oe, all shown in Fig. 35. Domain magnetizations return to the sample plane (two dimensional) after the field is increased beyond -20 Oe. The center magnetic flux stripe is wider and has higher contrast at negative saturation

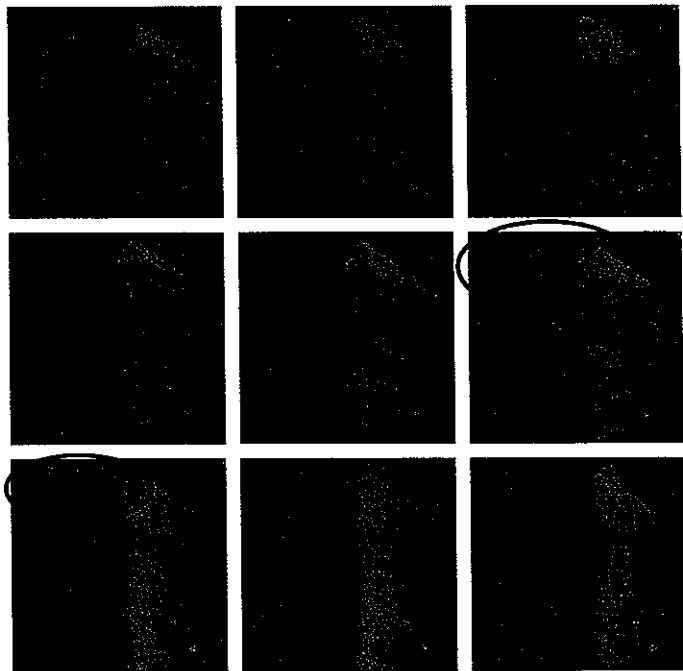


Fig. 35: Magnetic force microscope images $8 \mu\text{m}$ square of a section of tunnel junction, with NiFe free layer electrode on the left and junction multilayer stack on the right. Applied magnetic field strengths are, from left to right and top to bottom, 30, 9.9, 6.1, 3.7, 1.8, -2.8, -7.9, -14.1, and -42.5 Oe. Possible rotating vortex domain wall is circled.

Also of note is a possible vortex at the ellipsoid tip, and a flux closure path between the CoFe layer and NiFe free layer showing varying contrast based on the magnetization direction between the layers.

Specifically, as the field becomes more negative from positive saturation, small, three dimensional

than at positive, and almost disappears at during the transition. As the field reverses toward the positive direction, the nucleation process essentially reverses. The 3-D domains first appear in the free layer electrode and disappear last in the junction stack, and the dark flux line reappears along the physical edge at saturation. One significant difference is a larger scale domain boundary that moves toward the ellipsoid end as the field increases.

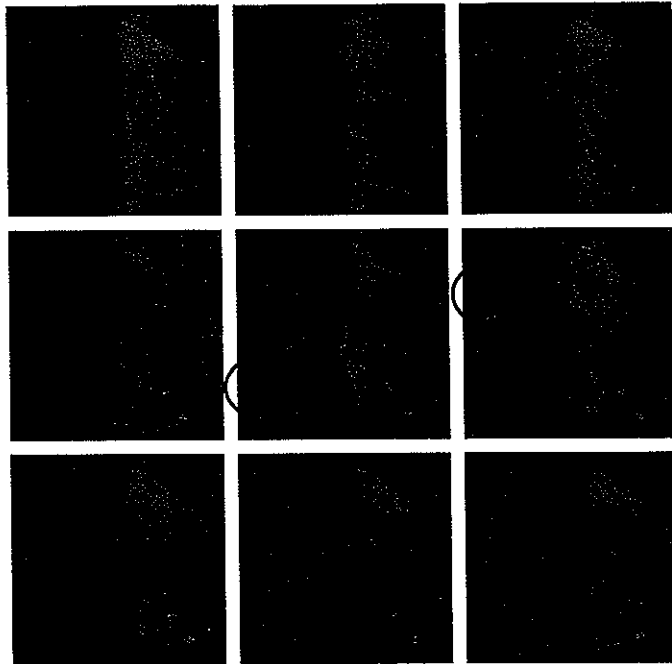


Fig. 36: Magnetic force microscope images $8\ \mu\text{m}$ square of a section of tunnel junction, with NiFe free layer electrode on the left and junction material stack on the right. Applied magnetic field strengths are, from left to right and top to bottom, -20.5, -10.5, -4.5, 1.5, 3.5, 5.5, 7.2, 11.6, and 29.5 Oe. Vortex and large-scale wall are circled.

4. DISCUSSION

4.1 CASE STUDY 1: Stress in an FeSiAl Thin Film Resulting in Striped Domains

Figure 20 shows the MFM images obtained from the same area of the 0% pp N sample at various stages of the hysteresis cycle. After the sample had been magnetized to saturation, on reducing the applied field a fine and irregular stripe domain structure nucleated (Fig. 20b). The stripe domains coarsened and became more regular as the applied field was reduced to zero (Fig. 20c). Along the steepest part of the hysteresis loop local switching of image contrast occurred, leading to connection and disconnection of the stripe domains (Figs. 20c-d). This suggests that the perpendicular magnetization component of parts of the stripe domains reversed. During this stage irreversible changes of the in-plane magnetization component also took place as indicated in the measured hysteresis loop. It was noticed that in this stage the domain width remained relatively constant and that independent switching of image contrast of parts of a stripe domain were observed. These observations seem to suggest that the irreversible changes of the in-plane component occurred mainly by local switching of domain magnetization or by local motion of short sections of domain wall. This may be accompanied by switching of the perpendicular component that was manifested as switching of the image contrast. This magnetization reversal process is different from that brought about by simultaneous motion of long domain wall sections. In the latter case, domains of the preferred magnetization direction would be observed to grow at the expense of neighboring domains as domain walls moved. Growing areas of the uniform MFM image contrast would be observed. This is contrary to the present observation that the stripe domain persisted and the domain width remained unchanged. The persistence of the stripe domain pattern could be due to the fact that the magnetostatic energy associated with it is lower than that of a

uniformly magnetized domain that has a uniform perpendicular component.

As the reverse field was increased beyond the coercive field the stripe domains disintegrated into short and irregular segments ($<0.5 \mu\text{m}$, Fig. 20e). An interpretation of the observed change is that the process consists of local switching of domain magnetization of a few grains into the film plane (the grain size was measured to be about $0.1 \mu\text{m}$ by TEM). This process is hysteretic as indicated in the high-field regime (from about 1.2 to 16 kA/m) of the magnetization curve. The domain width was found to decrease when the applied field was increased beyond the coercive point as a result of the disintegration of the stripe domains. Similar variations in stripe domain width with applied field in the high field regime have been observed in previous studies on other Fe-based thin films [22, 23]. Further increases of the applied field caused the image contrast to decrease as the in-plane magnetization along the field direction increased toward saturation (Fig. 20f).

Similar sequences of changes in MFM images were observed in the nitrated films.

Nevertheless several differences in magnetization reversal between the 0% pp N film and the 1%–4% pp N films were noticed. For comparison the MFM images taken from the 3% pp N film are shown in Fig. 21. In the 3% pp N film a stripe domain structure was nucleated at a higher field than in the 0% pp N film (compare Fig. 21a with 20a). A larger reverse field was needed for domain switching to take place in the 3% pp N film than in the 0% pp N film, showing that domain wall pinning is stronger in the former. Similar behavior was observed in the 1, 2, and 4% pp N films. These observations are consistent with the results of the VSM measurements which show that the 1%–4% pp N films had higher coercivities than the 0% pp N film.

The domain reversal of 5% and 10% pp N films exhibited subtle differences from that observed in the 0%–4% pp N films. As shown in Fig. 22, after stripe domains were nucleated (Fig. 22b) the domain pattern of the 5% pp N film exhibited smaller changes (Figs. 22c and 22d) than in the 0%–4% pp N films along the steepest part of the hysteresis loop. As the reverse field was increased beyond the coercive field the bright stripes became wider than the dark stripes. No disintegration of the stripe domains was observed when the sample magnetization approached saturation. Similar domain reversal was found in the 10% pp N film. This observation is in contrast to that made on the 0%–4% pp N films. A possible explanation is that in the high field regime the magnetization process taking place in the 5% and 10% pp N films involved mainly uniform rotation of domain magnetization towards the sample plane, while in the 0%–4% pp N films local switching of domain magnetization occurred instead.

Evidence of strong domain wall pinning was actually observed in the 0%–4% pp N films. An example is given in Figs. 23(a) and 23(b) which shows the MFM images obtained from the 0% pp N sample at oppositely magnetized remanent states. Regions with complementary image contrast were observed. This indicates strong domain wall pinning, probably at the grain boundaries, as the domain width was of the same order of magnitude as the grain size (~ 400 nm versus ~ 250 nm, respectively). This suggestion is supported by the fact that strong domain wall pinning was not observed in the 5%–10% pp N samples. As shown in Figs. 23(c) and 23(d), the stripe domain structures found in the 5% pp N sample at the oppositely magnetized remanent states show much less repetition than in the 0% pp N sample. The observed difference in domain pinning between the two groups of films (namely the 0%–4%

films, and the 5%–10% pp N films) could be related to the change in the film structure as pp N was increased from 4% to 5%. It was found in the TEM study that the 0%–4% pp N films have large columnar bcc grains ($\sim 0.1 \mu\text{m}$), while the 5% and 10% pp N films consist of a mixture of randomly oriented equiaxed bcc nanograins (10 nm diameter or less) in an amorphous matrix (Fig. 18). Since the grains in the 5% and 10% pp N films are much smaller than the domain width, the effect of ripple and the strength of domain wall pinning are weaker than in the 0%–4% pp N films.

This data all correlates with the shapes of the VSM loops in figures 20-22, with the local switching at hysteretic field points and coherent rotation along the sloped regions of the loop, as seen in the corresponding figures and as discussed above.

4.2 CASE STUDY 2: Magnetization reversal in CoFeHfO films

As seen in Fig. 24 the easy axis hysteresis loops of both the thick CoFeHfO film and the thin coated film exhibit high squareness, suggesting by themselves that the magnetization reversal involves mostly irreversible domain wall motion across the films with very little domain rotation. The hard axis loops of both films indicate the opposite, with most of the magnetization reversal likely brought about by domain rotation. This conclusion agrees well with the domain patterns of Fig. 25 in which all observed changes were in local switching of regions about $0.2 \mu\text{m}$ in size, and to the domain patterns observed in the thicker film. Both of these changes occurred near their respective coercive fields, as would be expected. The lack of change as the field is further increased in either direction also correlates to the VSM picture of the film magnetization.

The imagery along the hard axis of the thicker film showed little either in the way of domain switching as in Fig. 25 or in changes in image contrast as in Fig. 26. Thus the magnetization reversal in this film probably involved coherent rotation of domains in the sample plane, which is usually expected in films with an in-plane uniaxial anisotropy under hard-axis applied fields. This sample can then be said to match the VSM loop predictions of domain behavior quite well. However, the drastic contrast changes and domain changes seen in the thinner CoFeHfO film (Fig. 26) are less easily explained. The domain pattern likely corresponds to the formation of magnetic ripples caused by local variations in anisotropy [24]. Adjacent domains would have anti-parallel magnetization components along the easy axis but parallel magnetization components in the applied field direction. Increasing the hard-axis field causes the domain magnetization to rotate toward the field direction in all three dimensions, leading to a maximum in contrast when the in plane components of the magnetic moments could lie along the energetically favorable easy axis. During this rotation, the contrast increases and decreases as seen in the micrographs.

4.3 CASE STUDY 3: Anisotropy in a Complex Magnetic Material

The rosette domain patterns visible in Fig. 27b and Fig. 37 are unique to a specific group of materials – ferromagnets with a relatively high, uniaxial anisotropy. While the stripes in Fig. 27a may seem to contradict this, these stripes are consistent with a small angular shift of the b-axis ($\sim 3^\circ$) as the crystal transitions from monoclinic phase to orthorhombic phase. As the samples were cut with specific axes normal to the sample plane at room temperature, the face of the ferromagnetic low temperature phase would no longer be parallel to the b-c plane of

the crystal structure. When both of these images are compared to Kerr images of a NdFeB single crystal (Fig. 37), the magnetic moment alignment of the $\text{Gd}_5(\text{Si}_2\text{Ge}_2)$ single crystals becomes quite clear, even without comparison with the VSM data. These domain structures are a result of large domains aligned along the b-axis in the bulk crystal. The domains near the surface of the crystal begin to branch into smaller domains to minimize surface stray field energy as seen in the side plane Kerr image in Fig. 37. When viewed with the easy axis of the crystal perpendicular to the surface, these branches appear as the rose patterns seen in NdFeB, cobalt, other uniaxial materials, and now this complex gadolinium-silicon-germanium material. This conclusion is in marked contrast to the a- or c-axis anisotropy expected of this material and to related Tb_5Si_4 and Tb_5Ge_4 compounds, as mentioned above. In fact, this bulk magnetic structure is counter-intuitive given the crystal structure illustrated in Fig. 11. It implies that the magnetic exchange of the Gd ion moments is not between Gd nearest neighbors in the a-c slabs as might be anticipated, but instead is indirect, propagating perpendicular and along interplanar (Si, Ge)—(Si, Ge) bonds. Despite this conceptual difficulty with the results, they are strongly substantiated by the VSM results on one single crystal in Fig. 30 and are compatible with the significant increase in interplanar Si—Ge bonding in the ferromagnetic phase from the monoclinic phase.

The peculiar patterns observed in the high purity polycrystalline samples in Fig. 28 could also be interpreted in terms of the presence of a strong magnetic anisotropy. When the easy direction is inclined at an acute angle to the surface normal, the domains in the bulk have a magnetization component normal to the surface. The branching seen in the single crystal samples would therefore occur near the polycrystalline surface as well.

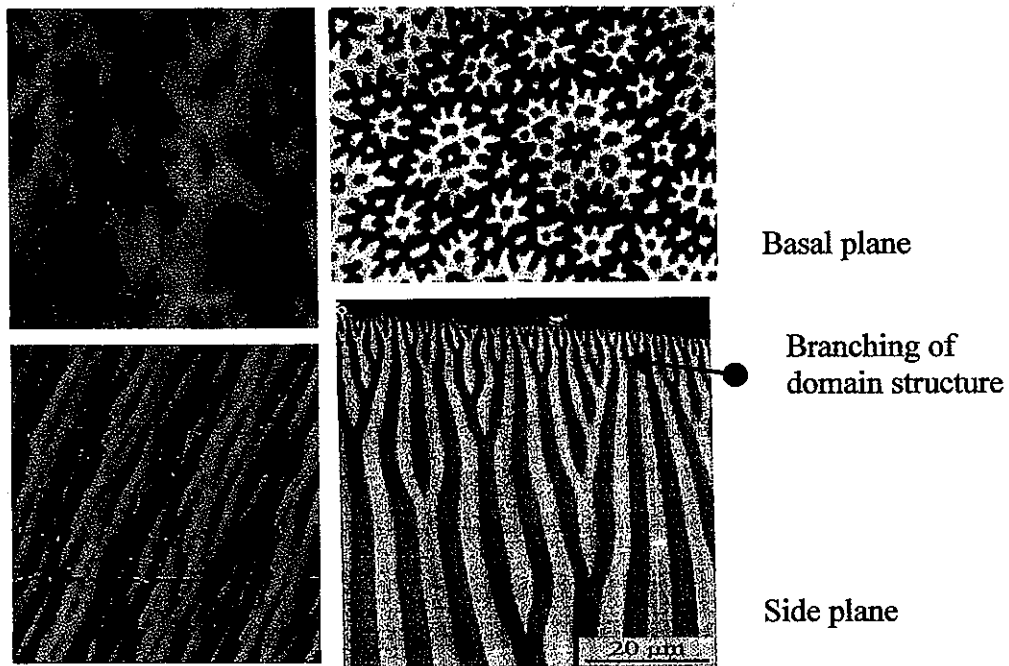


Fig. 37: Side-by-side comparison of MFM images of b-axis and a-axis $Gd_5(Si_2Ge_2)$ images (top and bottom left, $20 \mu m$ square) and Kerr images of basal and side planes of NdFeB single crystals.

As the temperature was lowered through the transition, the length scale of the domains might increase as the bulk-scale magnetic ordering increased. This is supported by thermal expansion studies at the phase transformation, which indicate a smaller range of temperature over which the transition occurs, and hence sharper order-disorder transitions in these same single crystal samples than in the polycrystalline sample [20].

4.4 CASE STUDY 4: Melt-spun $Fe_{75}Si_{10}B_{15}$ Ribbons

These ribbons also show a stripe domain structure when stressed (Fig. 31-33). When this structure is combined with the dendritic branching of the stripes (similar to the branching discussed in the case of the Gd-Si-Ge material), it is quite clear that, in this case, the tensile stress has pushed the anisotropy out of the ribbon plane. As seen in each figure, as the

degree of deformation increases, the contrast, stripe width, and stripe branching all change toward structures indicative of a strong out-of-plane anisotropy.

4.5 CASE STUDY 5: Magnetic Tunnel Junction Behavior

The line of dark contrast at the edge of the junction stack (Fig. 33, 35 and 36) indicates a strong spatial gradient of the magnetic field. The reason for such a state is that the magnetic flux path through the CoFe pinned layer either looped into the NiFe free layer (if the two dimensional configuration is antiparallel) or was repelled by the NiFe free layer (parallel configuration). This is supported by the disappearance of the line during switching of the junction and by the measured resistance of the junction device. The contrast is strongest when the antiparallel configuration drives a higher resistance and weaker when the parallel configuration drives a lower resistance. See images 1, 6, and 9 of Fig. 35 for representative examples.

Between $\pm H_C$, smaller domains with higher stray field indicate a complicated rotation mechanism for the moments in the free layer. The larger domains seen at higher fields do not rotate coherently; they nucleate, rotate independently and often out of the sample plane, and then recombine to form larger domains again in the oppositely magnetized state. These patterns are caused by the combined effects of applied magnetic field, magnetic anisotropy, and magnetostatic effects of the pointed ellipsoidal shape, the straight edge of the multilayer stack, the thin-film aspect ratio of each electrode, and the layers and their domain walls on each other. The magnetization change of the free layer is clearly not caused by simple

rotation or flipping. In fact, each reversal sequence shows a domain structure that might be a vortex (see circled regions in Fig. 35 and 36).

It should be noted that the behavior of the domains exhibited in Fig. 36 appears to match the behavior modeled for tapered ellipsoids and show similarities to “domain wall traps” modeled by McMichael et. al. [25]. The shapes are intended to nucleate domains near the center of the ellipse and allow for domain wall travel toward the ends under increasing applied field, which occurs on a longer length scale in the center three images of Fig. 36 (smaller scale domains disappear in a line from bottom to top). In the last image there is a sustained light contrast, much like the domain configuration modeled for the traps, which are of dimensions $\sim 0.5\mu\text{m} \times \sim 0.25\mu\text{m}$. Qualitatively, then, the behavior of this larger junction can serve as a model for smaller, device-sized junctions.

5. CONCLUSIONS

In the first case study involving the FeSiAl thin films, contrast and spacing of domain patterns are clearly related to microstructure and stress. As would be expected from magnetomechanical calculations, the greater the stress, the greater the perpendicular anisotropy. This is clearly seen from the increase in contrast and saturation field as the stress of the film increases (all are maximums in the 3% film). Microstructure seems to contribute most strongly to local site pinning of domains. The VSM loops for these samples can, then, be easily explained.

Case study #2 most clearly demonstrates localized, incoherent domain wall motion switching with field applied along an easy axis for a square hysteresis loop. The thicker CoFeHfO film, in fact, appeared to demonstrate expected coherent rotation behavior for the hard axis as well. However, hard axis images of the thinner film, with their unexpected perpendicular rotation behavior, demonstrate how localized imaging of domains can be almost uncorrelated to the bulk behavior of a material.

In case study #3, axis-specific images of the complex Gd-Si-Ge material clearly show the influence of uniaxial anisotropy. These MFM images qualitatively predicted the VSM measurements quite well, as proven by the anisotropy calculations performed. In effect, the images quantitatively reflect the anisotropy coefficients to within an order of magnitude, as the type of patterns seen in Fig. 27 are characteristic to materials with uniaxial anisotropy coefficient K_1 within about an order of magnitude to 10^4 J/m^3 .

Case study #4, the only study with the sole intent of creating domain structures for imaging, also demonstrated in fairly simple terms the effects of increasing stress on domain patterns. These ribbons also show a striped domain pattern when stressed, and when combined with dendritic branching of the stripes, the images again indicate that the anisotropy of the ribbon has been pushed out of the ribbon plane. Contrast and properties of stripes change with degree of deformation up to the point seen in Fig 31. The pattern seen highlighted in this figure even begins to qualitatively match the rosettes seen in the $\text{Gd}_5(\text{Si}_2\text{Ge}_2)$ single crystal.

In case study #5, it was proven that the width of magnetoresistance loops could be quantitatively predicted using only MFM. However, the magnitude of the resistance change can not be predicted, as the nature of the in-plane magnetizations of the electrode layers cannot be measured using MFM. It may be possible, then, to combine Kerr or TEM domain imaging with MFM to predict all qualities of an MR loop. The “squareness” of hysteresis was shown to be directly related to the switching of smaller domains between parallel and antiparallel states, a process that may be more characteristic of similar large junctions than smaller junctions used in memory arrays and other products. The longer scale domain behavior of this junction does, however, seem to correlate with modeling of smaller junctions, as noted in the discussion above.

When all case studies are considered together, a dominating factor seems to be that of anisotropy, both magnetocrystalline and stress induced. Any quantitative bulk measurements heavily reliant on K coefficients, such as the saturation fields for the FeSiAl films, H_C in cases 1, 3, and 5, and the uniaxial character of the $\text{Gd}_5(\text{Si}_2\text{Ge}_2)$, transferred to and from the

domain scale quite well. *In-situ* measurements of domain rotation and switching could also be strongly correlated with bulk magnetic properties, including coercivity, M_S , and hysteresis loop shape. In most cases, the qualitative nature of the domain structures, when properly considered, matched quite well to what might have been expected from theory and calculation, and provided such information in a matter of minutes. In fact, typical characterization in each of these studies was far more complete and reliable with domain imagery to back it up – especially the single crystal and applied field pictures. In these simple cases, it appears that domain imagery may be close to standing alone in magnetic characterization. The surprises in the 10 nm CoFeHfO film, the complexity seen in the polycrystalline Gd-Si-Ge sample and the broad range predictions of the K_1 of the same reinforce the unreliability of making concrete statements based purely on domain imagery of any type, but it may be possible to create standards similar to the types used in optical microscopy for metallography in these complex cases.

6. WORKS CITED

- [1] Jiles, David. *Introduction to Magnetism and Magnetic Materials: 2nd Edition*.
London: Chapman & Hall, 1998.
- [2] Langevin, P. *Ann. Chem. Et Phys.*, **5**, 70, 1905.
- [3] Weiss, P., Foex., G. *Le Magnetisme*, Paris: Armand Colin, 1926.
- [4] Bitter, F. *Phys. Rev.*, **38**, 1903-1905 (1931).
- [5] A. Hubert and R. Schafer, *Magnetic Domains: The Analysis of Magnetic
Microstructures*. Berlin: Springer-Verlag, 2000, pp. 401-406.
- [6] Martin, Y., Wickramasinghe, H.K. *Appl. Phys. Lett.*, **50**, 1455-1457 (1987).
- [7] "Veeco Products – Find By Market – Scientific & Industrial Research." www.di.com
(April 5, 2003).
- [8] P. M. Dodd, R. Atkinson, P. Papakonstantinou, M. S. Araghi, and H. S. Gamble, *J.
Appl. Phys.* **81**, 4104 (1997).
- [9] M. I. Ullah, K. R. Coffey, M. A. Parker, and J. K. Howard, *IEEE Trans. Magn.* **30**,
3927 (1994).
- [10] D. Macken, P. Scullion, and K. Duddy, *J. Appl. Phys.* **87**, 6517 (2000).
- [11] P. M. Dodd, R. Atkinson, I. W. Salter, M. S. Araghi, and H. S. Gamble, *J. Appl.
Phys.* **85**, 4559 (1999).
- [12] Y. Hayakawa, K. Ohminato, N. Hasegawa, and A. Makino, *J. Phys, IV*, **7**, 1155-
4339 (1997).
- [13] V.K. Pecharsky and K.A. Gschneidner, Jr., *Adv. Mater*, **13**, 683 (2001), and
references therein.
- [14] K.S. Kim, S.C. Yu, H.B. Lee, and Y.K. Kim, *J. Magn. and Magn. Mater.*, **239**, 1-3,

- 560-563 (2002).
- [15] J.S. Moodera, L.R. Kinder, T.M. Wong, and R. Meservey, *Phys. Rev. Lett.* vol. 74, 3273-3276 (1995).
- [16] J.S. Moodera and G.Mathon, *J. Magn. Magn. Mater.*, vol. 200, pp. 248-273, 1999.
- [17] J. Leib, C.C.H. Lo, J.E. Snyder, and D.C. Jiles, *J. Appl. Phys.*, **93**, no. 10, 2003.
- [18] Proceedings of the 5th M4 Conference, Ames, Iowa, 2002.
- [19] D. Wang, Non Volatile Electronics, Eden Prairie, Minnesota, personal communication, 2002.
- [20] J. Leib, J.E. Snyder, C.C.H. Lo, J.A. Paulsen, P. Xi and D.C. Jiles. *J. Appl. Phys.*, **91**, no.10, 2002.
- [21] S. Chikazumi, *Physics of Ferromagnetism*. Oxford: Clarendon, 1997, pp. 491-4
- [22] H. S. Cho, V. R. Inturi, J. A. Barnard, and H. Fujiwara, *IEEE Trans. Magn.* **34**, 1150 (1998).
- [23] S. Foss, C. Merton, R. Proksch, G. Skidmore, J. Schmidt, E. D. Dahlberg, T. Pokhil, and Y.-T. Cheng, *J. Magn. Magn. Mater.*, **190**, 60 (1998).
- [24] M. Prutton, *Thin Ferromagnetic Films*. London: Butterworths, 1964, pp. 164-167.
- [25] R.D. McMichael, J. Eicke, M.J. Donahue, and D.G. Porter, *J. Appl. Phys.*, **87**, no. 9, 2000, p. 7058.

APPENDIX: COPIES OF PUBLICATIONS AND PAPERS



ELSEVIER

Journal of Magnetism and Magnetic Materials 226-230 (2001) 1669-1671



www.elsevier.com/locate/jmmm

The effect of nitrogen on the microstructure, stress, and magnetic properties of RF-sputtered FeSiAl(N) thin films

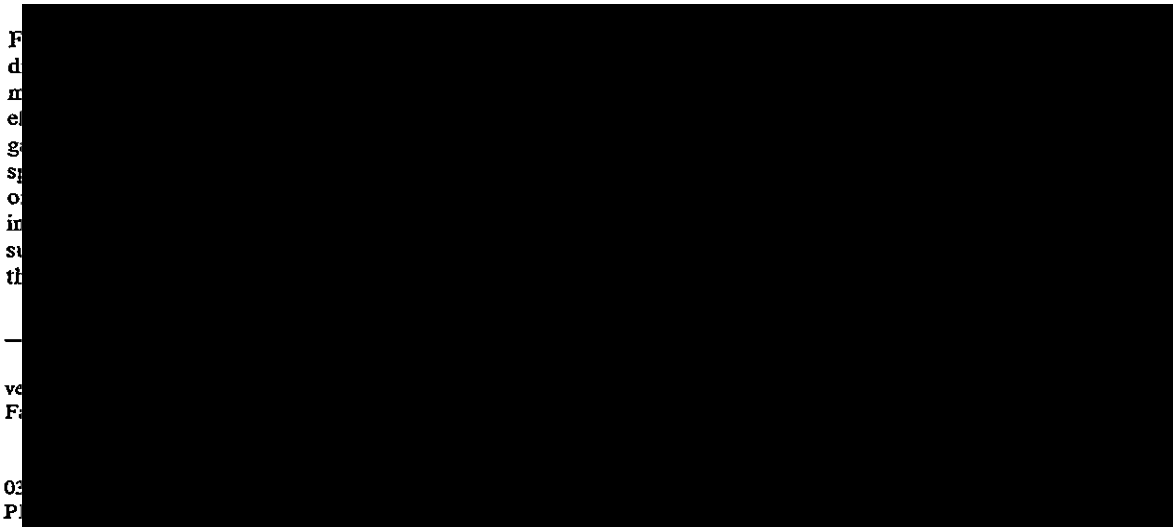
J.E. Snyder^{a,b,*}, C.C.H. Lo^a, R. Chen^{a,c}, B. Kriegermeier-Sutton^{a,b}, J. Leib^{a,b},
S.J. Lee^a, M.J. Kramer^{a,b}, D.C. Jiles^{a,b,c}, M.T. Kief^d

^aAmes Laboratory, USDoE, Iowa State University, Ames, IA 50011, USA

^bMaterials Science and Engineering Department, Iowa State University, Ames, IA 50011, USA

^cDepartment of Electrical and Computer Engineering, Iowa State University, Ames, IA 50011, USA

^dSeagate Technology, Minneapolis MN 55435, USA



Magnetic force microscopy study of magnetization reversal in sputtered FeSiAl(N) films

C. C. H. Lo^{a)}

Ames Laboratory, United States Department of Energy, Ames, Iowa 50011

J. E. Snyder and J. Leib

Ames Laboratory, United States Department of Energy, Ames, Iowa 50011 and Materials Science and Engineering Department, Iowa State University, Ames, Iowa 50011

R. Chen

Ames Laboratory, United States Department of Energy, Ames, Iowa 50011 and Department of Electrical and Computer Engineering, Iowa State University, Ames, Iowa 50011

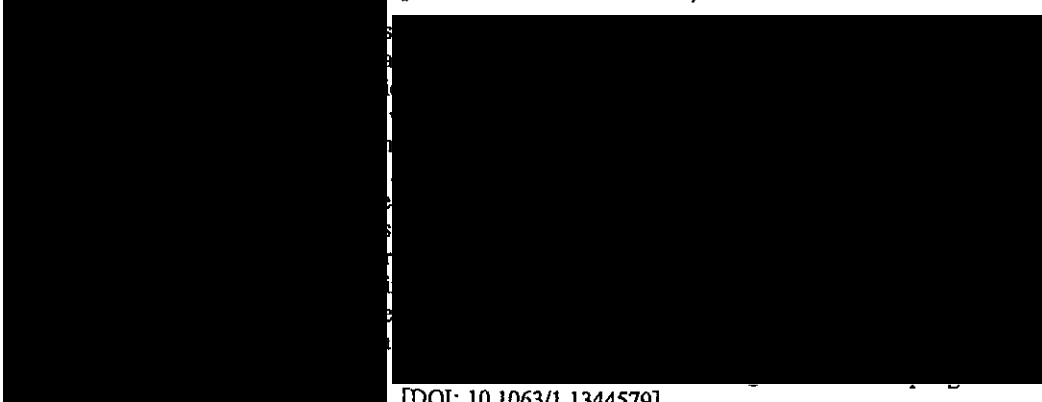
B. Kriegemeier-Sutton, M. J. Kramer, and D. C. Jiles

Ames Laboratory, United States Department of Energy, Ames, Iowa 50011 and Materials Science and Engineering Department, Iowa State University, Ames, Iowa 50011

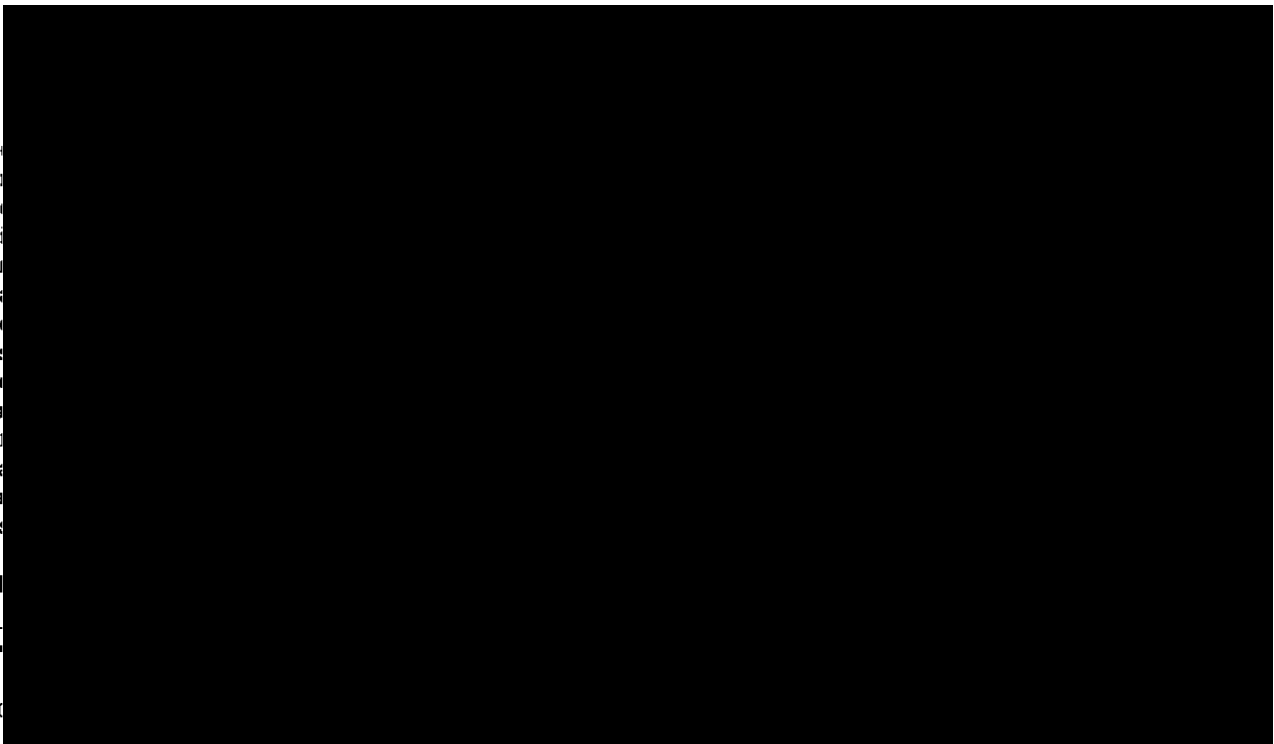
M. T. Kief

Seagate Technology, Minneapolis, Minnesota 55435

(Received 6 October 2000; accepted for publication 1 December 2000)



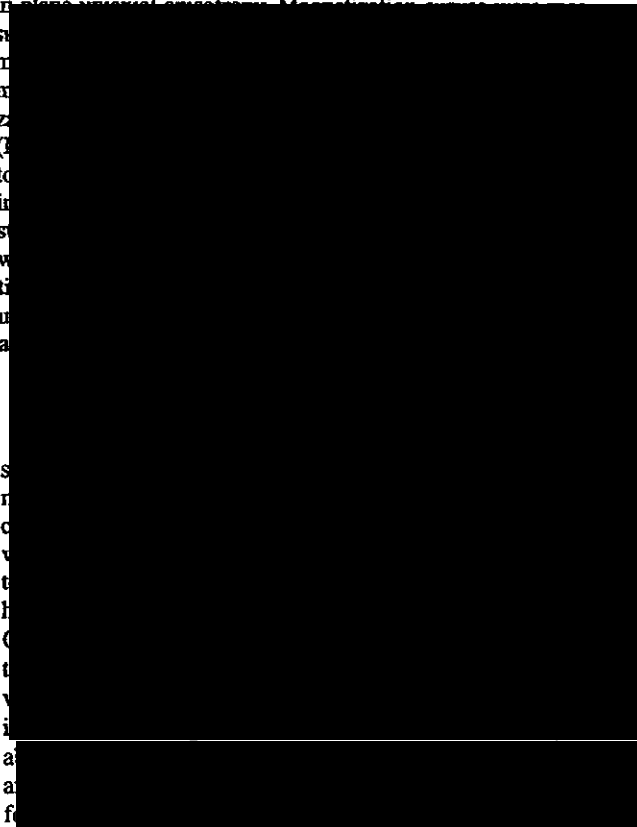
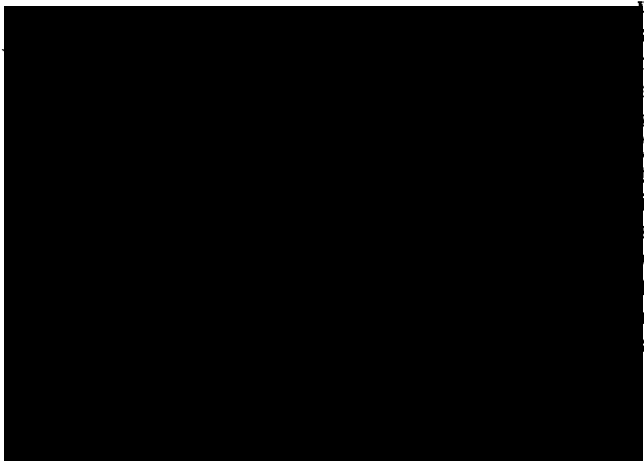
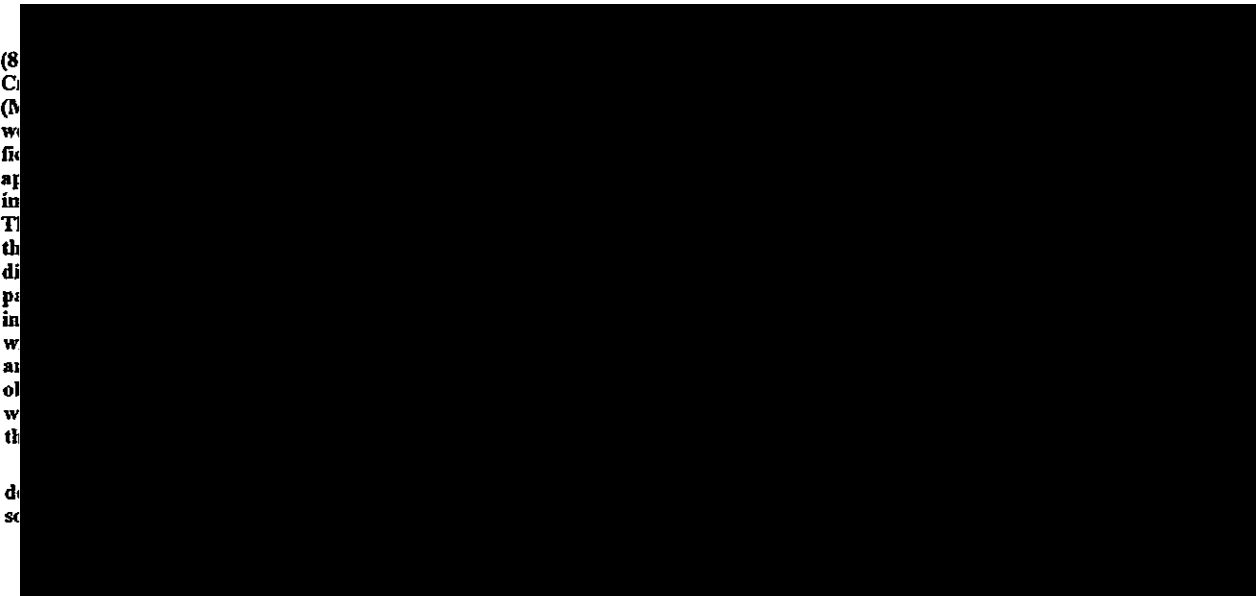
[DOI: 10.1063/1.1344579]



Magnetization Reversal in CoFeHfO Films

C. C. H. Lo, *Member, IEEE*, J. E. Snyder, *Senior Member, IEEE*, J. Leib, D. Wang, Z. Qian, J. M. Daughton, *Fellow, IEEE*, and D. C. Jiles, *Fellow, IEEE*

(8
C
(M
w
fi
ap
in
T
th
di
pa
in
w
an
ol
w
th
d
sc



Manuscript received October 12, 2000.

This work was supported by the U.S. Department of Energy, Office of Basic Energy Sciences, under Contract W-7405-Eng-82. The authors from NVE were supported by NSF under Contract DMI-9961165, and the National Institute of Standards and Technology (NIST) of US Department of Commerce, under both the Advanced Technology Program (ATP) Cooperative Agreement Number 70NANB8H 4025 and Contract 50-DKNB-0-90087.

C. C. H. Lo is with Ames Laboratory, USDoE, Iowa State University, Ames, IA 50011 USA (e-mail: clo@iastate.edu).

J. E. Snyder, J. Leib, and D. C. Jiles are with Ames Laboratory, USDoE, and Materials Science and Engineering Department, Iowa State University, Ames, IA 50011 USA.

D. Wang, Z. Qian, and J. M. Daughton are with Nonvolatile Electronics, Inc., 11409 Valley View Road, Eden Prairie, MN 55344 USA.

Publisher Item Identifier S 0018-9464(01)06779-6.



Magnetic force microscopy characterization of a first-order transition: Magnetic-martensitic phase transformation in $\text{Gd}_5(\text{Si}_x\text{Ge}_{1-x})_4$

J. Leib^{a)} and J. E. Snyder

Ames Laboratory, Iowa State University, Ames, Iowa 50011 and Department of Materials Science and Engineering, Iowa State University, Ames, Iowa 50011

C. C. H. Lo and J. A. Paulsen

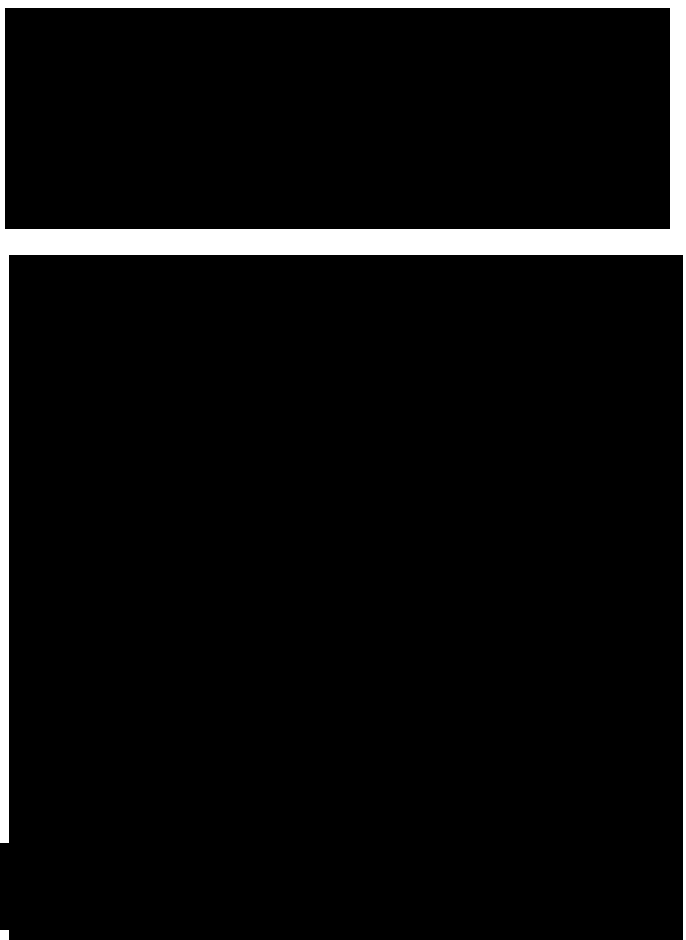
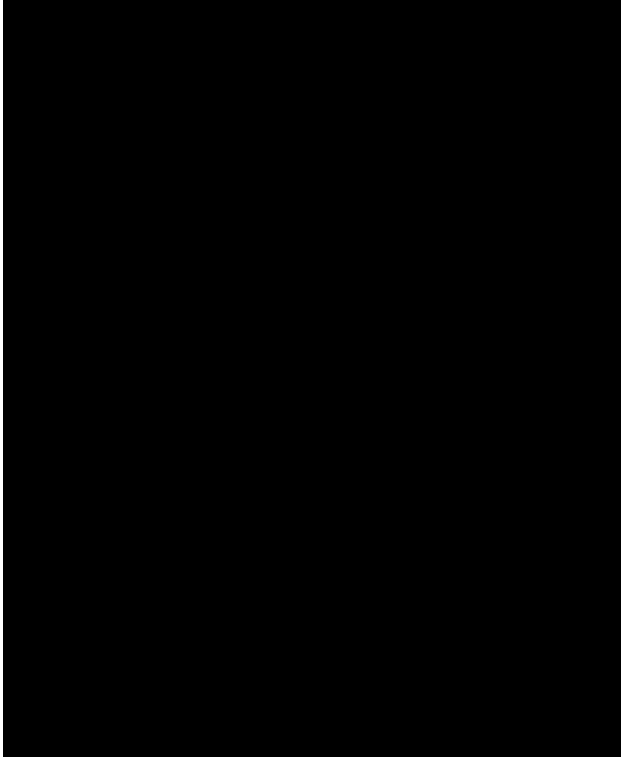
Ames Laboratory, Iowa State University, Ames, Iowa 50011

P. Xi and D. C. Jiles

Ames Laboratory, Iowa State University, Ames, Iowa 50011 and Department of Materials Science and Engineering, Iowa State University, Ames, Iowa 50011



[DOI: 10.1063/1.1456059]

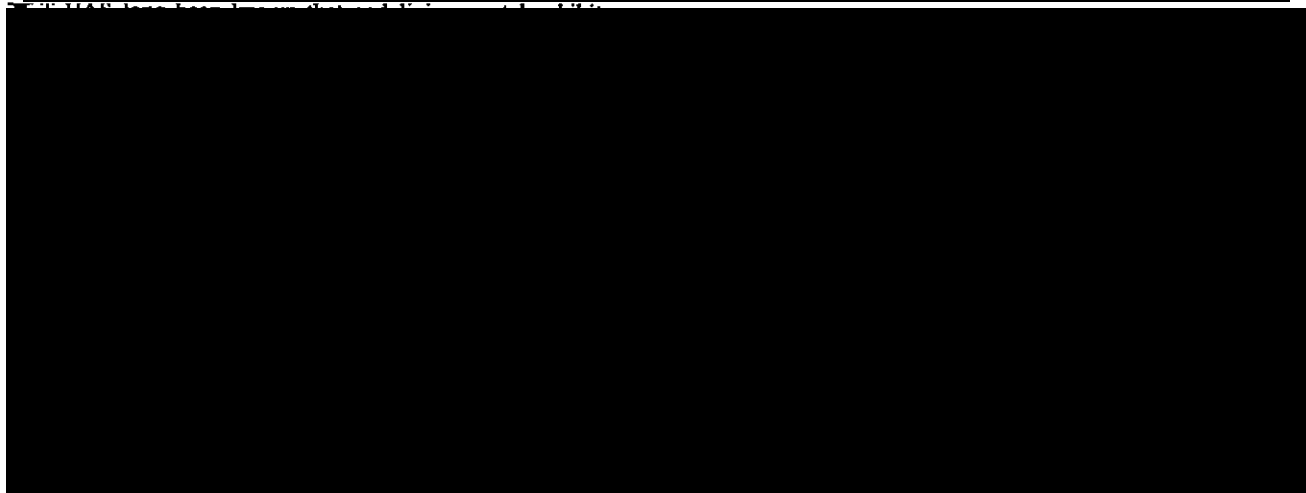
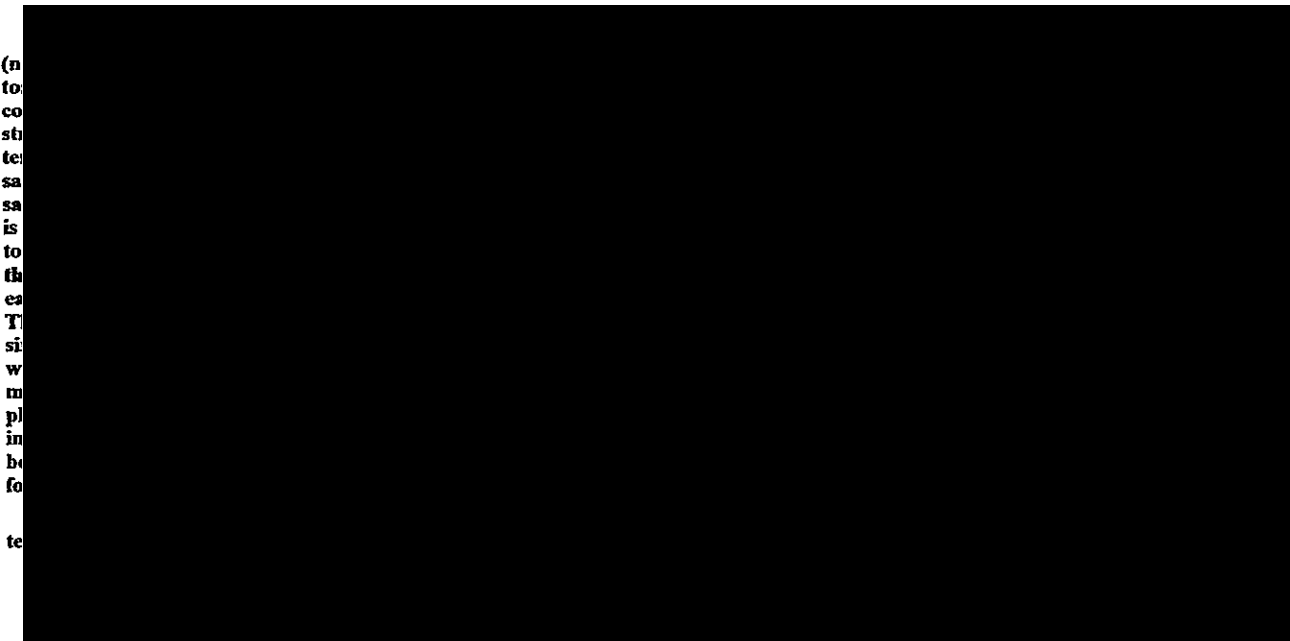


^{a)}Electronic mail: jleib@iastate.edu

Magnetic Force Microscopy Characterization of Unusual Magnetic Coupling in an Extraordinarily Responsive Magnetic Material

J. S. Leib, *Student Member, IEEE*, C. C. H. Lo, *Member, IEEE*, J. E. Snyder, *Senior Member, IEEE*,
D. C. Jiles, *Fellow, IEEE*, V. K. Pecharsky, D. S. Schlagel, and T. A. Lograsso

(n
to
co
st
te
sa
is
to
th
es
T
si
w
m
pl
in
be
fo
te



Manuscript received February 14, 2002; revised May 28, 2002. This work was supported by the U.S. Department of Energy, Office of Basic Energy Sciences, Materials Sciences Division, under Contract W-7405-Eng-82.

The authors are with the Metals and Ceramics Sciences Division, Ames Laboratory, Iowa State University, Ames, IA 50011 USA (e-mail: gauss@ameslab.gov).

Digital Object Identifier 10.1109/TMAG.2002.803587.



Thermal expansion studies on the unusual first order transition of $Gd_5Si_{2.09}Ge_{1.91}$: effects of purity of Gd

M. Han;^{1,2} D. C. Jiles;^{1,2,4} J. E. Snyder;^{1,2} C. C. H. Lo;¹ J. S. Leib;^{1,2} J. A. Paulsen;^{1,3}
T. A. Lograsso;¹ and D. L. Schlage¹

¹Metal & Ceramics Sciences Division, Ames Laboratory, U.S. Department of Energy, Ames, IA 50011.

²Department of Materials Science & Engineering, Iowa State University, Ames, IA 50011.

³Department of Mechanical Engineering, Iowa State University, Ames, IA 50011.

⁴Department of Electrical and Computer Engineering, Iowa State University, Ames, IA 50011.

(Presented on 15 November 2002)

Two polycrystalline samples were made by using high purity Gd and commercial Gd, respectively, but with Si and Ge starting materials of the same purity in both cases. Thermal expansion results showed that both samples exhibited a first order phase transformation, with a discontinuity in thermally-induced strain and with hysteresis in the Curie temperature. Magnetic force microscopy has been used to demonstrate the magnetic phase transformation process from paramagnetic to ferromagnetic upon cooling. It was found that the Curie temperature was lower and the thermally-induced strain higher, in the sample made from lower purity level Gd starting materials compared with the sample made from high purity Gd metal. These results indicate that the impurities (mainly C, O, N, and F) in the Gd starting material can significantly alter the strain and Curie temperature of $Gd_5(Si_xGe_{1-x})_4$ alloys. © 2003 American Institute of Physics.
[DOI: 10.1063/1.1540060]

Introduction

The properties of $Gd_5(Si_xGe_{1-x})_4$ were first studied in 1967 (Holtzberg *et al.* 1967). In recent years, this material has attracted much attention due to its unusual giant magnetocaloric effect (MCE) (Pecharsky and Gschneidner, Jr. 1997), giant magneto-resistance (GMR), and colossal magnetostriction (CMS) (Pecharsky and Gschneidner, Jr. 2001). It is very unusual for a single material to possess these three effects together. The magnetocaloric effect is a phenomenon on which the alignment of randomly oriented magnetic moments caused by application of an external magnetic field results in heating, while randomizing the magnetic moments by removing the magnetic field results in cooling. Previous results indicated that the impurities in starting Gd material play a critical role in determining the magnitude of the giant MCE in the final material (Gschneider, Jr. *et al.* 2000). In this study, the effect of impurities on the magnetoelastic properties of $Gd_5(Si_xGe_{1-x})_4$ system is also reported through the measurement of thermal expansion. The results show that the strain amplitude is higher in the material made from lower purity Gd.

Experimental Details

Two polycrystalline $Gd_5(Si_{2.09}Ge_{1.91})$ samples were prepared by arc-melting a stoichiometric mixture of pure components in an argon atmosphere under normal pressure. The two samples used the same purity Si and Ge starting materials (both >99.99 at.%). One of the samples was prepared using Ames Laboratory (AL) Gd(99.8% pure), the major impurities (in atomic ppm) of which were: 440-O, 200-C, 160-H. Sample 2 was fabricated by using commercial purity Gd (96.9 at.% pure) which contained 18300-O, 4300-C,

4300-N, and 3700-F (in atomic ppm). Mass losses after arc-melting were less than 0.5 wt.%, so the alloy chemical compositions were assumed to be, to a first approximation, unchanged in the final product. The thermal expansion measurements were conducted using the strain-gauge method in a Janis Research 2-stage closed cycle helium refrigeration. The sample was cooled down from room temperature through the Curie point transition, and then later was heated up through the Curie point transition. The linear thermal expansion was measured during both cooling and heating. The Curie temperatures was determined by differentiating the cooling and heating curves and finding the maximum derivative of the strain with respect to temperature. In addition, a magnetic field $B=1$ T was applied along the measurement direction to study the effect of magnetic field on the magnetoelastic properties. *In situ* magnetic force microscopy (MFM) was used to observe the phase transformation. This was carried out by using an MFM equipped with a heating-cooling stage.

Results and Discussion

Thermal expansion measurement results are shown in Fig. 1 for the sample $Gd_5(Si_{2.09}Ge_{1.91})$ made from AL Gd at $B=0$ and 1 T. An abrupt change in strain was observed at 283 K on cooling and 288 K on heating for $B=0$ T; and at 287.5 K on cooling and 298 K on heating for $B=1$ T. A discontinuity in thermal strain and thermal hysteresis are signatures of a first-order phase transition. Above the transition temperature, the sample is paramagnetic and monoclinic. Below the transition temperature, it is ferromagnetic and orthorhombic. Previous references have indicated that this first order coupled magnetic-crystallographic transition only occurs within the composition range (Pecharsky and

In situ applied field imaging of a magnetic tunnel junction using magnetic force microscopy

J. Leib*

Department of Materials Science and Engineering, Iowa State University, Ames, Iowa and Ames Laboratory, U.S. Department of Energy, Ames, Iowa

C. C. H. Lo

Ames Laboratory, U.S. Department of Energy, Ames, Iowa

J. E. Snyder and D. C. Jiles

Department of Materials Science and Engineering, Iowa State University, Ames, Iowa and Ames Laboratory, U.S. Department of Energy, Ames, Iowa

(Presented on 15 November 2002)

Knowledge of domain behavior in magnetic tunnel junctions is an essential component, together with knowledge of the electron band structure, for understanding their magnetoelectronic properties. To this purpose, the magnetization reversal processes of a multilayer tunnel junction of structure substrate/NiFe/AIO₂/FeCo/CrPtMn/Al of tapered half-ellipsoid shape have been imaged using a magnetic force microscope (MFM) with *in situ* applied magnetic fields. Stripe domains through both the stack and free layers observed at zero applied field were erased by a ~ 100 Oe field applied to the left followed by applying a small field to the right. Magnetic domain structure did not reappear in the MFM images until a field of ~ 400 Oe was applied to the right. This domain pattern then persisted when the magnetic field was reduced to zero. A drastic difference in domain patterns throughout the rotational processes to saturation in each direction was also observed. When the field was applied to the left, domain walls rotated toward the direction perpendicular to the applied field before disappearing. However, in near-saturation fields to the right, domain walls formed nearly parallel to the applied field and rotated away from parallel as the applied field strength was decreased. From these images, therefore, significant insight has been gained into the magnetization processes and physical phenomena behind the magnetoresistive behavior of these junctions.
© 2003 American Institute of Physics. [DOI: 10.1063/L1540128]

I. INTRODUCTION

Magnetic tunnel junctions (MTJ's) that show magnetoresistance at room temperature were first observed in 1995 by Moodera and co-workers,¹ and fabricated by photolithographical techniques at NonVolatile Electronics in 1996.² MTJ's are a topic of great current scientific and engineering interest.³ The phenomena involved and the potential applications are both of significant interest. MTJ's pass a tunneling current from one ferromagnetic electrode through an insulating layer into a second ferromagnetic electrode, and this current depends on spin-dependent tunneling. The resistance of the junction depends on the relative directions of the magnetization in the two ferromagnetic electrodes as well as on the occupancy of majority and minority spin half bands. The magnetoresistive response of MTJ's depends on switching of the magnetization of the magnetic layers under an externally applied field, the details of which even now have not been fully addressed. The aim of this work is to investigate the magnetization reversal processes in MTJ's through direct observation of the domain wall processes using magnetic force microscopy (MFM) with *in situ* applied field capability.

*Electronic mail: jleib@iastate.edu

II. EXPERIMENTAL METHODS

The MTJ's with a multilayer structure consisting of substrate/NiFe(120)-AlO₂(15)-FeCo(54)-CrPtMn(328)-Al(54) (Fig. 1, all dimensions in angstroms) were deposited at NonVolatile Electronics on a Si wafer and patterned into a variety of devices for investigation. The junction studied was chosen for its large size (to ease MFM imaging) and its relatively large distance from other magnetic structures on the wafer (to reduce unwanted interactions and interference). It was patterned into a tapered half-ellipsoidal shape with dimensions of ~ 12 μm at the widest point along the short axis and ~ 40 μm along the long axis, with the bottom NiFe free layer a full ellipsoid. A magnetic anisotropy was induced in the NiFe layers, with the easy direction of magnetization along the short axis of the ellipsoid. A magnetic force microscope (Digital Instruments, Inc., Dimension 3100) was used in this research, employing magnetic probes (Digital Instruments, Inc., MESP) coated with CoCr. The MFM was equipped with an electromagnetic stage capable of applying variable magnetic fields up to ± 600 Oe to the junction *in situ* in the sample plane. The applied field was monitored using a Hall probe embedded in the magnetizing stage. Images were taken at several constant applied fields over three-quarters of a typical hysteresis loop starting with an initial magnetiza-

STUDIES ON THE EFFECTS OF PULSED-MAGNETIC FIELD TREATMENT ON MAGNETIC MATERIALS

M.J. Johnson¹, L.C. Kerdus¹, C.C.H. Lo¹, J.E. Snyder^{2,3}, J. Leib², S.J. Lee³, M. Mina⁴ and D.C. Jiles^{1,2,3,4}

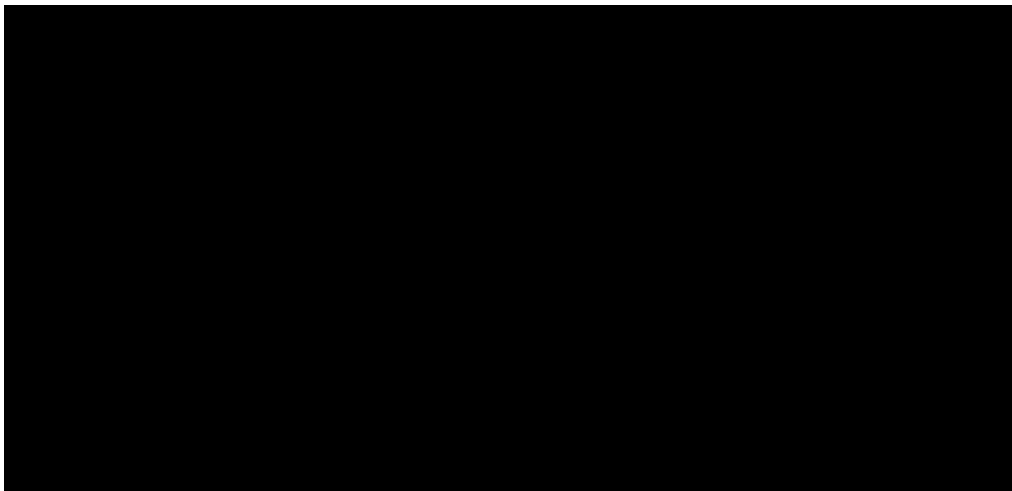
¹*Center for NDE, Iowa State University, Ames, IA 50011, USA*

²*Department of Materials Science and Engineering, Iowa State University, Ames, IA 50011, USA*

³*Ames Laboratory, USDoE, Ames, IA 50011, USA*

⁴*Department of Electrical and Computer Engineering, Iowa State University, Ames, IA 50011, USA*

Abstract. We have carried out systematic studies to investigate the effects of pulsed-magnetic field treatment on the residual stresses of carbon steels, nickel and magnetic thin film samples. A test bed was constructed for complete control of the magnetic field profile. The magnetic properties and stress states of the samples were measured before and after the treatment. Results indicate that the magnetic treatment does not have any detectable effects on the stress state of the samples.



MAGNETIC FIELD GRADIENT MEASUREMENT ON MAGNETIC CARDS USING MAGNETIC FORCE MICROSCOPY

C.C.H. Lo¹, J. Leib², D.C. Jiles^{1,2} and W.C. Chedister³

¹*Center for NDE, Iowa State University, Ames, Iowa 50011, USA*

²*Department of Materials Sciences and Engineering, Iowa State University, Ames, IA 50011, USA*

³*Circle Systems, Inc, Hinckley, IL 60520, USA*

Abstract. The magnetic field gradients of magnetic stripe cards, which are developed for classifying magnetic particles used in magnetic particle inspections, have been measured using a magnetic force microscope (MFM). The magnetic force exerted on a MFM probe by the stray field emanating from the card was measured to determine the field gradients. The results are in good agreement with the field gradients estimated from the magnetizing field strengths used in the encoding process.

